12-2018

Finite Element Discretizations for Linear Elasticity

Emma Cinatl
Clemson University, mathgirl1024@gmail.com

Finite Element Discretizations for Linear Elasticity

A Thesis
Presented to
the Graduate School of
Clemson University

In Partial Fulfillment
of the Requirements for the Degree
Master of Science
Mathematical and Statistical Sciences

by
Emma Cinatl
December 2018

Accepted by:
Dr. Timo Heister, Committee Chair
Dr. Leo Rebholz
Dr. Hyesuk Lee

Abstract

The elasticity equations describe how an elastic material moves under a force. An elastic material is one that returns to its original shape after the force is lifted. Modeling elasticity is useful in manufacturing applications such as suspension cables and nail bending, and biological applications such as weight on bones and tendons [1].

In this thesis we study the modeling of nearly incompressible linearly elastic materials. A *nearly incompressible* material is one that does not change much under pressure. Linearly elastic materials exhibit small deformations under a force. Standard finite element methods do not work well on nearly incompressible materials when using the simplest form of the linear elasticity equations (the pure displacement form). Instead, they exhibit *locking*; in other words, they produce excessively small displacements on a coarse mesh.

We examine several methods that fix this problem. One method is to use a different form of the linear elasticity equations that more closely resembles a Stokes' formulation (the displacement-pressure formulation). This approach has theoretical support, but is somewhat computationally expensive. Another method is to use reduced integration for part of our equation. This approach has less theoretical support, but with the correct setups, this method is both cheaper and more accurate than the standard method, and solves the locking problem.

Table of Contents

Dedication

This thesis is dedicated to Justin Sybrandt. I can't possibly say thank you enough for all of your support, love, understanding, and delicious lasagna. You were always there for me no matter what, and it means the world to me.

I also want to thank all my friends for their support and late-night companionship, and to especially thank everyone who bought me the ergonomic keyboard I needed to type this thesis (Todd Morra, Justin Sybrandt, Peter Westerbaan, Anna Marie Vagnozzi, and Scott Scruggs). You are all wonderful people.

Chapter 1

Introduction

The goal of this paper is to compare and contrast the use of different finite element discretizations for the linear elasticity equations. We will first derive the weak form of the pure displacement formulation of the linear elasticity equations:

$$\begin{cases} \text{Seek } \mathbf{u} \in V_{DN} := \{\mathbf{v} \in [H^1(\Omega)]^d : \ \mathbf{v}|_{\partial\Omega_D} = 0\} \text{ such that} \\ a(\mathbf{u}, \mathbf{v}) = \int_\Omega \mathbf{f} \cdot \mathbf{v} + \int_{\partial\Omega_N} \mathbf{g} \cdot \mathbf{v} \text{ for all } \mathbf{v} \in V_{DN} \end{cases}$$

$$\text{where } a(\mathbf{u}, \mathbf{v}) = \int_\Omega \lambda(\text{div } \mathbf{u})(\text{div } \mathbf{v}) + \int_\Omega 2\mu\varepsilon(\mathbf{u}) : \varepsilon(\mathbf{v}).$$

We next discuss the Galerkin method of discretizing our problem and several polynomial spaces we use for our test functions. We also present the displacement-pressure formulation of the linear elasticity equations:

$$\begin{cases} 2\mu \int_\Omega \varepsilon(\mathbf{u}) : \varepsilon(\mathbf{v}) - \int_\Omega p \cdot \text{div } \mathbf{v} = \int_\Omega f \cdot \mathbf{v} & \text{for all } \mathbf{v} \in [H_0^1(\Omega)]^d \\ -\int_\Omega q \cdot \text{div } \mathbf{u} - \frac{1}{\lambda} p \cdot q = 0 & \text{for all } q \in [L^2(\Omega)]^d \end{cases}$$

We next introduce the problem of *locking* that occurs when using the standard finite elements Q_1 and Q_2 on the pure-displacement formulation. Using these elements to model incompressible materials with Neumann conditions yields inaccurate solutions on coarse meshes and sub-optimal error rates [2, 3, 4, 5, 6, 7].

Some reduced-integration schemes solve this problem of locking [4]. Two such schemes introduced in this paper we term Q_1-midpoint and Q_2-gauss2, which we base on the standard elements Q_1 and Q_2, respectively. We under-integrate the term $\lambda \int_\Omega (\text{div } \mathbf{u})(\text{div } \mathbf{v})$ that appears in the weak form of our pure displacement formulation. [7, 4] take a similar approach. Using the displacement-pressure formulation of the equation also fixes locking [4]. Certain reduced-integration schemes can be shown to be equivalent to certain displacement-pressure-based discretizations. For example, our Q_1-midpoint method and the $Q_1 - dGP_0$ are equivalent [8]. Some other reduced-integration schemes work despite a lack of such an equivalence.

We modified the step-8 tutorial program [9] from the finite element library deal.II to explore our various methods. As is, the step-8 tutorial program solves the pure displacement form of the linear elasticity problem using linear basis elements, for Lamé parameter values $\lambda = \mu = 1$. We add to this basic formulation several reduced integration schemes and an implementation of the displacement-pressure formulation, as well as the necessary structure to easily try different values for the parameters λ, μ, and ν. We also add a manufactured solution and a Timoshenko benchmark from [10] to evaluate our methods. (A link to our code can be found in Appendix A.)

Finally, we compare the solutions and error rates obtained with each of our methods.

Chapter 2

Mathematical Background

Here we discuss elasticity, and derive the weak formulation of the pure displacement form of the linear elasticity equations (with mixed boundary conditions). We also present the displacement-pressure form of the linear elasticity equations, and introduce the Galerkin discretization scheme. (For notation, see Section 2.1.2.)

2.1 Linear Elasticity

2.1.1 Introduction to elasticity

We study the displacement field $\mathbf{u} : \Omega \to \mathbb{R}^d$ resulting from letting a medium originally at equilibrium reach a second equilibrium after applying an external load. We can picture this situation with Figure 2.1:

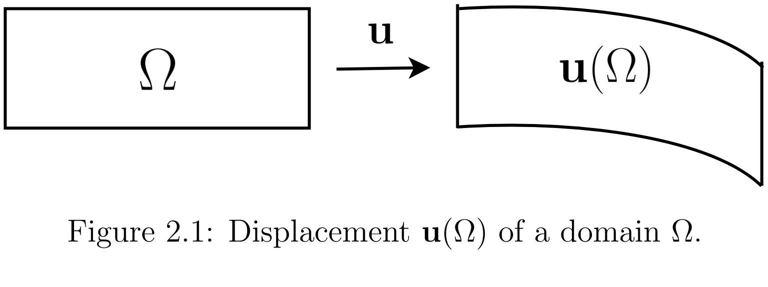

Figure 2.1: Displacement $\mathbf{u}(\Omega)$ of a domain Ω.

and write the deformed domain as $\mathbf{u}(\Omega) = \{\mathbf{u}(\mathbf{x}) : \mathbf{x} \in \Omega\}$. We call the external load applied to our medium $\mathbf{f} : \Omega \to \mathbb{R}^d$. Thus set up, elasticity theory is, in general, non-linear, and satisfies Hooke's Law

$$\sigma = C : \varepsilon$$

and the equilibrium equation

$$\text{div } (\sigma) + \mathbf{f} = 0$$

where σ is the Cauchy stress tensor, C is the fourth-order stiffness tensor, and ε is the strain tensor [11].

This thesis focuses on the more specific case of homogeneous linear isotropic materials. Under a force, isotropic materials deform the same way (relative to the direction of the force) regardless of the relative orientations of the force and the material. In other words, such a material reacts the "same" way to a force applied in different directions [12]. A homogeneous material has the same properties throughout. In other words, the material has the same composition at any given points [13]. Our assumption of linearity implies that subjecting our material to a force will result in infinitesimal strains, or equivalently, small deformations. Additionally, the stress and strain produced by subjecting the material to a force will be linearly related, i.e. $\sigma \sim \varepsilon$ [11].

In order to model linear elasticity, we need two parameters characterizing the material. We primarily use the Lamé parameters λ and μ, which together describe the compressibility of the material [2]. In the context of elasticity, μ represents the shear modulus of the material [14]. The parameter λ corresponds to the stresses resulting from density changes [3]. Thermodynamic stability requires $\mu > 0$ and $\lambda + \dfrac{2}{3}\mu \geq 0$, but for simplicity we assume that $\lambda \geq 0$, as does much of the literature [2, 15, 16, 3]. As is usually done with linear elasticity, we take μ and λ to be constants [2].

We then write the stress tensor of the deformed medium as $\sigma(\mathbf{u}) : \Omega \to \mathbb{R}^{d,d}$, written $\sigma(\mathbf{u}) = \left(\begin{smallmatrix} \sigma_{11} & \sigma_{12} \\ \sigma_{21} & \sigma_{22} \end{smallmatrix}\right)$ for $d = 2$ [2]. Specifically, we get the linear elasticity version of Hooke's Law [15]:

$$\sigma(\mathbf{u}) = \lambda(\text{div }\mathbf{u})I + 2\mu\varepsilon(\mathbf{u})$$

Our strain rate tensor $\varepsilon(\mathbf{u}) : \Omega \to \mathbb{R}^{d,d}$ for our deformed medium is

$$\varepsilon(\mathbf{u}) = \frac{1}{2}(\nabla\mathbf{u} + (\nabla\mathbf{u})^T).$$

2.1.2 Notation

We next introduce some useful mathematical operators, spaces, and norms. We spell out the element-wise definitions in two dimensions for the sake of simplicity.

Definition 2.1.1. *Given a vector field* $\mathbf{u} = \left(\begin{smallmatrix} u_1 \\ u_2 \end{smallmatrix}\right)$, *where* $\mathbf{u}$ *is a function of* x *and* y, *we denote by* u_{ix} *the partial derivative with respect to* x *of the* i*th component of* $\mathbf{u}$, *and by* u_{iy} *the partial derivative with respect to* y *of the* i*th component of* $\mathbf{u}$, *for* $i = 1, 2$.

Definition 2.1.2. *The* divergence *of a* d*-dimensional vector* $\mathbf{u}$ *is the scalar* $\text{div }\ \mathbf{u} := \sum_{i=1}^{d} u_{ii}$, *where* u_{ii} *is the derivative of the* i*th component with respect to* x_i.

Definition 2.1.3. *The* gradient *of a vector* $\mathbf{u}$ *is the tensor* $\nabla\mathbf{u} := \left(\begin{smallmatrix} u_{1x} & u_{1y} \\ u_{2x} & u_{2y} \end{smallmatrix}\right)$.

We give the following definitions in terms of a dimension d. In practice, as above, we will use the definitions with $d = 2$. We assume throughout that $\Omega \subset \mathbb{R}^d$ is a domain. We firstly introduce the L^2 space and related norms.

Definition 2.1.4. *The* L^2 *space of scalar-valued functions on some domain* $\Omega \subset \mathbb{R}^d$ *is* $L^2(\Omega) := \{u : \Omega \to \mathbb{R} : \int_\Omega u^2 < \infty\}$

Definition 2.1.5. *The L^2 norm on a scalar-valued function $u \in L^2(\Omega)$ is $\|u\|_{L^2(\Omega)} := (\int_\Omega u^2)^{\frac{1}{2}}$.*

Note that $L^2(\Omega)$ is a Hilbert space with the inner product $(u,v)_{L^2(\Omega)} := \int_\Omega uv$. [16]

Definition 2.1.6. *We denote by $[L^2(\Omega)]^d$ the space $L^2(\Omega) \times L^2(\Omega) \times \cdots \times L^2(\Omega)$ (d copies of $L^2(\Omega)$). Then, the L^2 norm of the vector-valued function $\mathbf{u} \in [L^2(\Omega)]^d$ is $\|\mathbf{u}\|_{[L^2(\Omega)]^d} := (\sum_{i=1}^d \|u_i\|_{L^2}^2)^{\frac{1}{2}}$.*

We secondly introduce the H^1 space and related norms.

Definition 2.1.7. *The H^1 space of scalar-valued functions on some domain $\Omega \subset \mathbb{R}^d$ is $H^1(\Omega) := \{u \in L^2(\Omega) : \nabla u \in L^2(\Omega)\}$.*

Definition 2.1.8. *The H^1 norm on a scalar-valued function $u \in H^1(\Omega)$ is*

$$\|u\|_{H^1(\Omega)} := (\|u\|_{L^2(\Omega)}^2 + \|\nabla u\|_{L^2(\Omega)}^2)^{\frac{1}{2}} = (\textstyle\int_\Omega (u^2 + (\nabla u)^2)^{\frac{1}{2}}.$$

Definition 2.1.9. *We denote by $[H^1(\Omega)]^d$ the space $H^1(\Omega) \times H^1(\Omega) \times \cdots \times H^1(\Omega)$ (d copies of $H^1(\Omega)$). Then, the H^1 norm of the vector-valued function $\mathbf{u} \in [H^1(\Omega)]^d$ is $\|\mathbf{u}\|_{[H^1(\Omega)]^d} := (\sum_{i=1}^d \|u_i\|_{[H^1(\Omega)]^d}^2)^{\frac{1}{2}}$.*

Note that $[H^1(\Omega)]^d$ is a Hilbert space with the inner product

$$(\mathbf{u}, \mathbf{v})_{[H^1(\Omega)]^d} = (\mathbf{u}, \mathbf{v})_{[L^2(\Omega)]^d} + (\nabla \mathbf{u}, \nabla \mathbf{v})_{[L^2(\Omega)]^d} \text{ [3].}$$

2.1.3 Strong form of the linear elasticity equations

We denote the part of our boundary with Dirichlet conditions as $\partial\Omega_D$, and the part of the boundary with Neumann conditions as $\partial\Omega_N$; in short, $\partial\Omega = \partial\Omega_D \cup \partial\Omega_N$. For the simplicity of the following arguments we assume the Dirichlet boundary conditions are homogeneous. An example depiction of this boundary setup is given in Figure 2.2:

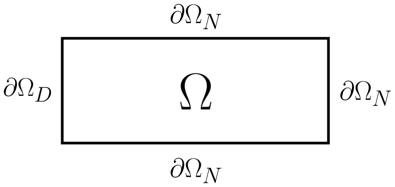

Figure 2.2: Boundary with part Dirichlet and part Neumann conditions imposed.

Our equations and assumptions above then give us the following **strong form of the linear elasticity equations** [2]:

Seek $\mathbf{u} : \mathbb{R}^d \to \mathbb{R}^d$ such that

$$\begin{cases} -\text{div } \sigma(\mathbf{u}) = \mathbf{f} & \text{in } \Omega \\ \sigma(\mathbf{u}) = \lambda(\text{div } \mathbf{u})I + 2\mu\varepsilon(\mathbf{u}) & \text{in } \Omega \\ \mathbf{u} = 0 & \text{on } \partial\Omega_D \\ \sigma(\mathbf{u}) \cdot \mathbf{n} = \mathbf{g} & \text{on } \partial\Omega_N \end{cases}$$

where $\mathbf{f}$ is the volume force applied on Ω and $\mathbf{g}$ is the normal force applied on $\partial\Omega_N$.

2.1.4 Derivation of the pure displacement weak form of the linear elasticity equations

In order to solve our system of equations for $\mathbf{u}$, we will follow the standard approach of multiplying parts of our system by a "test function" $\mathbf{v}$ from the function space $V_{DN} := \{\mathbf{v} \in [H^1(\Omega)]^d : \ v|_{\partial\Omega_D} = 0\}$ and then integrating both sides of our equation to get the "weak form" of the equations. We begin with a theorem from [17] and a few lemmas that we will need to derive and simplify our weak form.

Theorem 2.1.10. ***(Divergence Theorem.)*** *Let* $\mathbf{p}$ *and* $\mathbf{v}$ *be vector-valued functions, and let* $\mathbf{n}$ *be the normal vector on points of the boundary. Then* $\int_\Omega(\text{ div } \ \mathbf{p})\mathbf{v}+$

$\int_\Omega \mathbf{p} \cdot \nabla\mathbf{v} = \int_{\partial\Omega}(\mathbf{p}\cdot\mathbf{n})\mathbf{v}$.

Lemma 2.1.11. *Let $\sigma(\mathbf{u})$ be defined as above, and let $\mathbf{v}$ be a vector-valued function. Then $\sigma(\mathbf{u}) : \nabla\mathbf{v} = \sigma(\mathbf{u}) : \varepsilon(\mathbf{v})$.*

Proof. We present the proof in two dimensions for the sake of clarity, but the argument in three dimensions proceeds similarly.

Firstly, recall that div $\mathbf{u} =$ div $\left(\begin{smallmatrix} u_1 \\ u_2 \end{smallmatrix}\right) = u_{1x} + u_{2y}$, and note that

$$\varepsilon(\mathbf{u}) = \frac{1}{2}\Big(\nabla\left(\begin{smallmatrix} u_1 \\ u_2 \end{smallmatrix}\right) + \Big(\nabla\left(\begin{smallmatrix} u_1 \\ u_2 \end{smallmatrix}\right)\Big)^T\Big) = \frac{1}{2}\Big(\left(\begin{smallmatrix} u_{1x} & u_{1y} \\ u_{2x} & u_{2y} \end{smallmatrix}\right) + \left(\begin{smallmatrix} u_{1x} & u_{2x} \\ u_{1y} & u_{2y} \end{smallmatrix}\right)\Big) = \left(\begin{smallmatrix} u_{1x} & \frac{1}{2}(u_{1y}+u_{2x}) \\ \frac{1}{2}(u_{1y}+u_{2x}) & u_{2y} \end{smallmatrix}\right)$$

This gives us

$$\begin{aligned}
\sigma(\mathbf{u}) &= \lambda(\text{div }\mathbf{u})I + 2\mu\varepsilon(\mathbf{u}) \\
&= \left(\begin{smallmatrix} \lambda(u_{1x}+u_{2y}) & 0 \\ 0 & \lambda(u_{1x}+u_{2y}) \end{smallmatrix}\right) + \left(\begin{smallmatrix} 2\mu u_{1x} & \mu(u_{1y}+u_{2x}) \\ \mu(u_{1y}+u_{2x}) & 2\mu u_{2y} \end{smallmatrix}\right) \\
&= \left(\begin{smallmatrix} (\lambda+2\mu)u_{1x}+\lambda u_{2y} & \mu(u_{1y}+u_{2x}) \\ \mu(u_{1y}+u_{2x}) & \lambda u_{1x}+(\lambda+2\mu)u_{2y} \end{smallmatrix}\right)
\end{aligned}$$

so we obtain

$$\begin{aligned}
\sigma(\mathbf{u}) : \nabla\mathbf{v} = {} & ((\lambda+2\mu)u_{1x} + \lambda u_{2y})v_{1x} + (\mu(u_{1y}+u_{2x}))v_{1y} \\
& + (\mu(u_{1y}+u_{2x}))v_{2x} + (\lambda u_{1x} + (\lambda+2\mu)u_{2y})v_{2y}
\end{aligned}$$

and

$$\begin{aligned}\sigma(\mathbf{u}) : \varepsilon(\mathbf{v}) &= ((\lambda + 2\mu)u_{1x} + \lambda u_{2y})v_{1x} + (\mu(u_{1y} + u_{2x})) \cdot \frac{1}{2}(v_{1y} + v_{2x}) \\ &\quad + (\mu(u_{1y} + u_{2x})) \cdot \frac{1}{2}(v_{1y} + v_{2x}) + (\lambda u_{1x} + (\lambda + 2\mu)u_{2y})v_{2y} \\ &= ((\lambda + 2\mu)u_{1x} + \lambda u_{2y})v_{1x} + (\mu(u_{1y} + u_{2x}))v_{1y} \\ &\quad + (\mu(u_{1y} + u_{2x}))v_{2x} + (\lambda u_{1x} + (\lambda + 2\mu)u_{2y})v_{2y}\end{aligned}$$

Therefore, $\sigma(\mathbf{u}) : \nabla\mathbf{v} = \sigma(\mathbf{u}) : \varepsilon(\mathbf{v})$.

□

Lemma 2.1.12. *Let $\sigma(\mathbf{u})$ be defined as above, where $\mathbf{v}$ is a vector-valued function. Then $\sigma(\mathbf{u}) : \varepsilon(\mathbf{v}) = \lambda(\text{ div } \mathbf{u})(\text{ div } \mathbf{v}) + 2\mu\varepsilon(\mathbf{u}) : \varepsilon(\mathbf{v})$.*

Proof. Note that $I : \varepsilon(\mathbf{v}) = \text{div } \mathbf{v}$. Thus,

$$\begin{aligned}\sigma(\mathbf{u}) : \varepsilon(\mathbf{v}) &= (\lambda(\text{div } \mathbf{u})I + 2\mu\varepsilon(\mathbf{u})) : \varepsilon(\mathbf{v}) \\ &= \lambda(\text{div } \mathbf{u})I : \varepsilon(\mathbf{v}) + 2\mu\varepsilon(\mathbf{u}) : \varepsilon(\mathbf{v}) \\ &= \lambda(\text{div } \mathbf{u})(\text{div } \mathbf{v}) + 2\mu\varepsilon(\mathbf{u}) : \varepsilon(\mathbf{v})\end{aligned}$$

□

We are now ready to derive our weak form. Combining the Divergence Theorem and our two lemmas yields

$$\begin{aligned}\int_\Omega \mathbf{f}\cdot\mathbf{v} &= \int_\Omega -(\text{div }\sigma(\mathbf{u}))\cdot\mathbf{v}\\ &= \int_\Omega \sigma(\mathbf{u}) : \nabla\mathbf{v} - \int_{\partial\Omega} \mathbf{v}\cdot\sigma(\mathbf{u})\cdot n\\ &= \int_\Omega \sigma(\mathbf{u}) : \varepsilon(\mathbf{v}) - \int_{\partial\Omega} \mathbf{v}\cdot\sigma(\mathbf{u})\cdot n\\ &= \int_\Omega \lambda(\text{div }\mathbf{u})(\text{div }\mathbf{v}) + \int_\Omega 2\mu\varepsilon(\mathbf{u}) : \varepsilon(\mathbf{v}) - \int_{\partial\Omega} \mathbf{v}\cdot\sigma(\mathbf{u})\cdot n\end{aligned}$$

We can also simplify our boundary integral somewhat, by testing with functions $\mathbf{v}$ such that $\mathbf{v} = 0$ on $\partial\Omega_D$, and thus

$$\begin{aligned}\int_{\partial\Omega} \mathbf{v}\cdot\sigma(\mathbf{u})\cdot n &= \int_{\partial\Omega_D} \mathbf{v}\cdot\sigma(\mathbf{u})\cdot n + \int_{\partial\Omega_N} \mathbf{v}\cdot\sigma(\mathbf{u})\cdot n\\ &= \int_{\partial\Omega_D} 0\cdot\sigma(\mathbf{u})\cdot n + \int_{\partial\Omega_N} \mathbf{v}\cdot\sigma(\mathbf{u})\cdot n\\ &= \int_{\partial\Omega_N} \mathbf{v}\cdot\sigma(\mathbf{u})\cdot n\\ &= \int_{\partial\Omega_N} \mathbf{v}\cdot\mathbf{g}\end{aligned}$$

In the case where we have homogeneous Dirichlet conditions on part of the boundary and Neumann conditions on the other part, this leads us to the following **pure displacement weak formulation of the linear elasticity equations** [2]:

$$\begin{cases}\text{Seek } \mathbf{u}\in V_{DN} := \{\mathbf{v}\in[H^1(\Omega)]^d : \ \mathbf{v}|_{\partial\Omega_D} = 0\} \text{ such that}\\ a(\mathbf{u},\mathbf{v}) = \int_\Omega \mathbf{f}\cdot\mathbf{v} + \int_{\partial\Omega_N} \mathbf{g}\cdot\mathbf{v} \text{ for all } \mathbf{v}\in V_{DN}\end{cases} \tag{2.1}$$

$$\text{where } a(\mathbf{u},\mathbf{v}) = \int_\Omega \lambda(\text{div }\mathbf{u})(\text{div }\mathbf{v}) + \int_\Omega 2\mu\varepsilon(\mathbf{u}) : \varepsilon(\mathbf{v})$$

2.1.5 Well-posedness of the pure displacement weak form

To argue that our weak form is well-posed, we must first establish several definitions [18] and preliminary theorems [2, 16].

Definition 2.1.13. *A* bilinear form $a : [H^1(\Omega)]^d \times [H^1(\Omega)]^d \to \mathbb{R}$ *is a map such that for all* $\mathbf{u}_1, \mathbf{u}_2, \mathbf{u}, \mathbf{v}_1, \mathbf{v}_2, \mathbf{v} \in [H^1(\Omega)]^d$ *and for all* $c_1, c_2 \in \mathbb{R}$,

(i) $a(c_1 u_1 + c_2 u_2, \mathbf{v}) = c_1 a(u_1, \mathbf{v}) + c_2 a(u_2, \mathbf{v})$, *and*

(ii) $a(\mathbf{u}, c_1 v_1 + c_2 v_2) = c_1 a(\mathbf{u}, v_1) + c_2 a(\mathbf{u}, v_2)$.

Definition 2.1.14. *A bilinear form* $a : [H^1(\Omega)]^d \times [H^1(\Omega)]^d \to \mathbb{R}$ *is* bounded *if there exists* $C \in \mathbb{R}^+$ *such that* $a(\mathbf{u}, \mathbf{v}) \leq C\|\mathbf{u}\|_{[H^1(\Omega)]^d}\|\mathbf{v}\|_{[H^1(\Omega)]^d}$ *for all* $\mathbf{u}, \mathbf{v} \in [H^1(\Omega)]^d$.

With these definitions, we are ready for our definition of well-posedness from [2].

Definition 2.1.15. *A problem of the form*

$$\begin{cases} \text{Seek } \mathbf{u} \in W \text{ such that} \\ a(\mathbf{u}, \mathbf{v}) = f(\mathbf{v}) \,\forall\, \mathbf{v} \in V \end{cases}$$

where W *and* V *are Hilbert spaces, and* a *is a bounded bilinear form on* $W \times V$, *is* well-posed *if it has exactly one solution, and if there exists* $c \in \mathbb{R}^+$ *such that for all* $f \in H^-, ||\mathbf{u}||_W \leq c||f||_{H^-}$, *where* H^- *is the dual space of* H.

We still need several results before we can prove that our weak form is well posed.

Theorem 2.1.16. ***(Korn's Inequality.)*** *Let* $\Omega \subset \mathbb{R}^d$. *There exists* c *such that for all* $\mathbf{v} \in [H^1(\Omega)]^d$, $c\|\mathbf{v}\|_{[H^1(\Omega)]^d} \leq \|\varepsilon(\mathbf{v})\|_{[L^2(\Omega)]^d} + \|\mathbf{v}\|_{L^2(\Omega)}$.

This result and its proof can be found in [16].

Corollary 2.1.17. *Let $V_{DN} = \{\mathbf{v} \in [H^1(\Omega)]^d : \ v|_{\partial\Omega_D} = 0\}$, where the measure of $\partial\Omega_D > 0$. There exists a positive constant c such that $\|\varepsilon(\mathbf{v})\|_{[L^2(\Omega)]^d} \geq c\|\mathbf{v}\|_{[H^1(\Omega)]^d}$ $\forall \mathbf{v} \in V_{DN}$.*

Again, for the proof of this corollary, we refer the reader to [16].

Definition 2.1.18. *Let $a : [H^1(\Omega)]^d \times [H^1(\Omega)]^d \to \mathbb{R}$ be a bilinear form. Then a is* coercive *if there exists $\alpha \in \mathbb{R}^+$ such that $a(\mathbf{u}, \mathbf{u}) \geq \alpha\|\mathbf{u}\|^2_{[H^1(\Omega)]^d}$ for all $\mathbf{u} \in [H^1(\Omega)]^d$.*

Theorem 2.1.19. ***(Lax-Milgram Theorem.)*** *Let H be a given Hilbert space and $a : H \times H \to R$ be a bounded and coercive bilinear form with coercivity constant $\alpha \in \mathbb{R}^+$ and boundedness constant $C \in \mathbb{R}^+$. Also, let $F(v) := \int_\Omega \mathbf{f}\mathbf{v} \in H^-$, where H^- is the dual space of H. Then there exists a unique solution $\mathbf{u} \in H$ to the equation $a(\mathbf{u}, \mathbf{v}) = F(\mathbf{v})$ for all $\mathbf{v} \in H$. Moreover, $\|\mathbf{u}\|_H \leq \frac{1}{\alpha}\|F\|_{H^-}$.*

A proof of the Lax-Milgram Theorem is available in [16].

Lemma 2.1.20. *Let $\mathbf{u}$ be a d-dimensional vector field. Then $\varepsilon(\mathbf{u}) : \varepsilon(\mathbf{u}) \leq \nabla\mathbf{u} : \nabla\mathbf{u}$.*

Proof. We give the proof in two dimensions for the sake of clarity. The proof in three dimensions follows similarly. Note that

$$\varepsilon(\mathbf{u}) : \varepsilon(\mathbf{u}) = \begin{pmatrix} u_{1x} & \frac{1}{2}(u_{1y}+u_{2x}) \\ \frac{1}{2}(u_{1y}+u_{2x}) & u_{2y} \end{pmatrix} : \begin{pmatrix} u_{1x} & \frac{1}{2}(u_{1y}+u_{2x}) \\ \frac{1}{2}(u_{1y}+u_{2x}) & u_{2y} \end{pmatrix} = u_{1x}^2 + \frac{1}{2}(u_{1y}+u_{2x})^2 + u_{2y}^2$$

and $\nabla\mathbf{u} : \nabla\mathbf{u} = \begin{pmatrix} u_{1x} & u_{1y} \\ u_{2x} & u_{2y} \end{pmatrix} : \begin{pmatrix} u_{1x} & u_{1y} \\ u_{2x} & u_{2y} \end{pmatrix} = u_{1x}^2 + u_{1y}^2 + u_{2x}^2 + u_{2y}^2$, which gives us

$$\begin{aligned}\nabla\mathbf{u}:\nabla\mathbf{u}-\varepsilon(\mathbf{u}):\varepsilon(\mathbf{u}) &= u_{1x}^2+u_{1y}^2+u_{2x}^2+u_{2y}^2-(u_{1x}^2+\frac{1}{2}(u_{1y}+u_{2x})^2+u_{2y}^2)\\ &= u_{1y}^2+u_{2x}^2-\frac{1}{2}(u_{1y}^2+2u_{1y}u_{2x}+u_{2x}^2)\\ &= \frac{1}{2}u_{1y}^2-u_{1y}u_{2x}+\frac{1}{2}u_{2x}^2\\ &= \frac{1}{2}(u_{1y}-u_{2x})^2\geq 0\end{aligned}$$

Thus, $\varepsilon(\mathbf{u}):\varepsilon(\mathbf{u})\leq\nabla\mathbf{u}:\nabla\mathbf{u}$.

□

Lemma 2.1.21. *Let* $\mathbf{u}$ *be a d-dimensional vector field. Then* $(\text{ div }\ \mathbf{u})^2\leq d\nabla\mathbf{u}:\nabla\mathbf{u}$.

Proof. The three-dimensional proof is similar to the proof for $d=2$, which follows:

$$\begin{aligned}(\text{div }\mathbf{u})^2 &= (u_{1x}+u_{2y})^2\\ &\leq (u_{1x}+u_{2y})^2+(u_{1x}-u_{2y})^2\\ &= u_{1x}^2+2u_{1x}u_{2y}+u_{2y}^2+u_{1x}^2-2u_{1x}u_{2y}+u_{2y}^2\\ &= 2(u_{1x}^2+u_{2y}^2)\\ &\leq 2(u_{1x}^2+u_{1y}^2+u_{2x}^2+u_{2y}^2)\\ &= 2\nabla\mathbf{u}:\nabla\mathbf{u}\end{aligned}$$

. □

We are finally ready to prove that our pure displacement weak form is well-posed.

Theorem 2.1.22. *Assume that* $\partial\Omega_D$ *has non-zero measure, and that* $F(\mathbf{v})$ *is a bounded linear function in* V_{DN}^{-}. *Then the pure displacement weak form of the linear elasticity equations of (2.1) is well-posed.*

Proof. Note that our $a(\mathbf{u}, \mathbf{v})$ is bilinear. We assume that $\mathbf{f}$ and $\mathbf{g}$ are such that $F(\mathbf{v}) := \int_\Omega \mathbf{f} \cdot \mathbf{v} + \int_{\partial\Omega_N} \mathbf{g} \cdot \mathbf{v} \in V_{DN}^-$ and $F(\mathbf{v})$ is a bounded linear functional. We further assume that a non-trivial part of the boundary has homogeneous Dirichlet conditions.

We show that $a(\mathbf{u}, \mathbf{v}) = \int_\Omega \lambda(\text{div } \mathbf{u})(\text{div } \mathbf{v}) + \int_\Omega 2\mu\varepsilon(\mathbf{u}) : \varepsilon(\mathbf{v})$ is bounded. By the Cauchy-Schwarz Inequality, we know that $a(\mathbf{u}, \mathbf{v}) \leq (a(\mathbf{u}, \mathbf{u}))^{1/2}(a(\mathbf{v}, \mathbf{v}))^{1/2}$. Note that $a(\mathbf{u}, \mathbf{u}) = \int_\Omega \lambda(\text{div } \mathbf{u})^2 + \int_\Omega 2\mu\varepsilon(\mathbf{u}) : \varepsilon(\mathbf{u})$. Additionally, by Lemma 2.1.20 we have $\varepsilon(\mathbf{u}) : \varepsilon(\mathbf{u}) \leq \nabla\mathbf{u} : \nabla\mathbf{u}$, and Lemma 2.1.21 gives us $(\text{div } \mathbf{u})^2 \leq d\nabla\mathbf{u} : \nabla\mathbf{u}$. Thus,

$$\begin{aligned}
a(\mathbf{u}, \mathbf{u}) &= \int_\Omega \lambda(\text{div } \mathbf{u})^2 + \int_\Omega 2\mu\varepsilon(\mathbf{u}) : \varepsilon(\mathbf{u}) \\
&\leq \lambda \int_\Omega 2\nabla\mathbf{u} : \nabla\mathbf{u} + 2\mu \int_\Omega \nabla\mathbf{u} : \nabla\mathbf{u} \\
&= 2(\lambda + \mu) \int_\Omega \nabla\mathbf{u} : \nabla\mathbf{u} \\
&\leq 2(\lambda + \mu) \int_\Omega (\nabla\mathbf{u} : \nabla\mathbf{u} + \mathbf{u} \cdot \mathbf{u}) \\
&= 2(\lambda + \mu)(||u_1||_{H^1}^2 + ||u_2||_{H^1}^2) \\
&= 2(\lambda + \mu)||\mathbf{u}||_{[H^1(\Omega)]^d}^2
\end{aligned}$$

So we have

$$\begin{aligned}
a(\mathbf{u}, \mathbf{v}) &\leq (a(\mathbf{u}, \mathbf{u}))^{1/2}(a(\mathbf{v}, \mathbf{v}))^{1/2} \\
&\leq (2(\lambda + \mu)||\mathbf{u}||_{[H^1(\Omega)]^d}^2)^{1/2}(2(\lambda + \mu)||\mathbf{v}||_{[H^1(\Omega)]^d}^2)^{1/2} \\
&= 2(\lambda + \mu)||\mathbf{u}||_{[H^1(\Omega)]^d}||\mathbf{v}||_{[H^1(\Omega)]^d}
\end{aligned}$$

Therefore, $a(\mathbf{u}, \mathbf{v})$ is bounded.

We next show that $a(\mathbf{u}, \mathbf{v})$ is coercive. Since part of our boundary has homogeneous Dirichlet conditions and part has Neumann conditions, we can use Corollary 2.1.17 stated above. Then we have

$$a(\mathbf{u},\mathbf{u}) = \int_\Omega \lambda(\text{div }\mathbf{u}))^2 + 2\mu \int_\Omega \varepsilon(\mathbf{u}) : \varepsilon(\mathbf{u}) \geq 2\mu \int_\Omega \varepsilon(\mathbf{u}) : \varepsilon(\mathbf{u})$$
$$= 2\mu||\varepsilon(\mathbf{u})||^2_{[L^2(\Omega)]^d} \geq 2\mu c||\mathbf{u}||^2_{[H^1(\Omega)]^d} \text{ for some } c \in \mathbb{R}^+.$$

Thus, $a(\mathbf{u},\mathbf{v})$ is coercive.

Now that we have satisfied all the assumptions of the Lax-Milgram Theorem, we can apply it to our problem to conclude that there exists a unique solution $\mathbf{u} \in V_{DN}$ to the equation $a(\mathbf{u},\mathbf{v}) = F(\mathbf{v})$ for all $\mathbf{v} \in V_{DN}$. Moreover, $\|\mathbf{u}\|_{[H^1(\Omega)]^d} \leq \frac{1}{\alpha}\|F\|^{-}_{[H^1(\Omega)]^d}$. Thus our pure displacement weak formulation of the linear elasticity equations is well-posed. □

We note here that [3] states that the constant c arising from the use of Korn's equality is such that the coercivity constant α of $a(\mathbf{u},\mathbf{v})$ satisfies $\alpha = 2\mu c \leq \mu$. This will be a useful fact that we will reference later.

2.1.6 Displacement-pressure form of the linear elasticity equations

We introduce in this section the displacement-pressure formulation of the linear elasticity equations, since we will use this form for comparison later in this work.

Substituting a scalar unknown p (which can be identified with pressure) for $-\lambda\text{div }\mathbf{u}$ into the pure-displacement strong form yields the following **displacement-pressure strong form of the linear elasticity equations** [19]:

$$\begin{cases} -2\mu(\text{div }\varepsilon(\mathbf{u})) + \nabla p = f \\ \text{div }\mathbf{u} + \frac{1}{\lambda}p = 0 \end{cases} \tag{2.2}$$

This leads to the following **displacement-pressure weak form of the linear elasticity equations** with homogeneous Dirichlet boundary conditions [19]:

$$\begin{cases} 2\mu \int_\Omega \varepsilon(\mathbf{u}) : \varepsilon(\mathbf{v}) - \int_\Omega p \cdot \text{div } \mathbf{v} = \int_\Omega f \cdot v & \text{for all } v \in [H_0^1(\Omega)]^d \\ - \int_\Omega q \cdot \text{div } \mathbf{u} - \frac{1}{\lambda} p \cdot q = 0 & \text{for all } q \in L^2(\Omega) \end{cases}$$

The displacement-pressure formulation comes directly from the displacement formulation, which we have already proved is well-posed. [19] also gives us the well-posedness of the displacement-pressure formulation.

2.2 Finite Element Method

We have shown our weak forms above to be accurate and well-formulated. However, to actually solve them as they are, we would have to use an infinite number of test functions $\mathbf{v} \in V_{DN}$, since V_{DN} is an infinite-dimensional space. Clearly, this is computationally intractable. Instead, we apply the *Galerkin method* to discretize our weak form into a solvable form [20].

2.2.1 Galerkin Method

We choose an N-dimensional function space $V^h \subset V_{DN}$. We then solve for a discretized solution $\mathbf{u^h} \in V^h$ using test functions $\mathbf{v^h} \in V^h$ instead of the full space V_{DN}. Having a finite-dimensional function space allows us to choose a basis $\{\phi_\mathbf{1}, \phi_\mathbf{2}, ..., \phi_\mathbf{N}\}$ of V^h. Then, testing with all these basis functions ensures that our solution works for every function in V^h. Additionally, we can express our discretized solution as $\mathbf{u^h} := \sum_{j=1}^{N} U_j \phi_\mathbf{j}$, where $U_j, j = 1, ..., N$ are real-valued unknown coefficients. Then we can solve for these U_j's instead of $\mathbf{u}$ by using our setup so far to create a linear system using the following logic:

For each $i = 0, 1, ..., N$:

$$\begin{aligned}
&\lambda \int_\Omega (\text{div } \phi_\mathbf{i})(\text{div } \mathbf{u}^\mathbf{h}) + 2\mu \int_\Omega \varepsilon(\phi_\mathbf{i}) : \varepsilon(\mathbf{u}^\mathbf{h}) = \int_\Omega \mathbf{f}\phi_\mathbf{i} + \int_{\partial\Omega_N} \mathbf{g}\phi_\mathbf{i} \\
\Rightarrow &\lambda \int_\Omega (\text{div } \phi_\mathbf{i})\Big(\text{div } \sum_{j=1}^{N} U_j\phi_\mathbf{j}\Big) + 2\mu \int_\Omega \varepsilon(\phi_\mathbf{i}) : \varepsilon\Big(\sum_{j=1}^{N} U_j\phi_\mathbf{j}\Big) = \int_\Omega \mathbf{f}\phi_\mathbf{i} + \int_{\partial\Omega_N} \mathbf{g}\phi_\mathbf{i} \\
\Rightarrow &\lambda \sum_{j=1}^{N} \int_\Omega (\text{div } \phi_\mathbf{i})(\text{div } \phi_\mathbf{j})U_j + 2\mu \sum_{j=1}^{N} \int_\Omega \varepsilon(\phi_\mathbf{i}) : \varepsilon(\phi_\mathbf{j})U_j = \int_\Omega \mathbf{f}\phi_\mathbf{i} + \int_{\partial\Omega_N} \mathbf{g}\phi_\mathbf{i} \\
\Rightarrow &\sum_{j=1}^{N} \Big[\Big(\lambda \int_\Omega (\text{div } \phi_\mathbf{i})(\text{div } \phi_\mathbf{j}) + 2\mu \int_\Omega \varepsilon(\phi_\mathbf{i}) : \varepsilon(\phi_\mathbf{j})\Big)U_j\Big] = \int_\Omega \mathbf{f}\phi_\mathbf{i} + \int_{\partial\Omega_N} \mathbf{g}\phi_\mathbf{i}
\end{aligned}$$

This is a linear system $AU = F$, where $A_{ij} = \lambda \int_\Omega (\text{div } \phi_\mathbf{i})(\text{div } \phi_\mathbf{j}) + 2\mu \int_\Omega \varepsilon(\phi_\mathbf{i}) : \varepsilon(\phi_\mathbf{j})$, $F_i = \int_\Omega \mathbf{f}\phi_\mathbf{i} + \int_{\partial\Omega_N} \mathbf{g}\phi_\mathbf{i}$, and U consists of the unknowns U_j, $1 \leq j \leq n$.

2.2.2 Subdividing the domain into a mesh

To improve the accuracy of our approximations and lessen the computational expense, we subdivide our domain Ω into a mesh $\mathcal{T}_h$, and split our computations over each cell in the mesh. This allows a reasonable approximation of V_{DN} on each cell T of the mesh by a basis composed of lower-order functions. We construct our mesh $\mathcal{T}_h$ such that $\overline{\Omega} = \overline{\bigcup_{T \in \mathcal{T}_h} T}$ [21], where h is the maximum cell diameter.

Our work primarily uses conforming rectangular meshes such as the example in Figure 2.3.

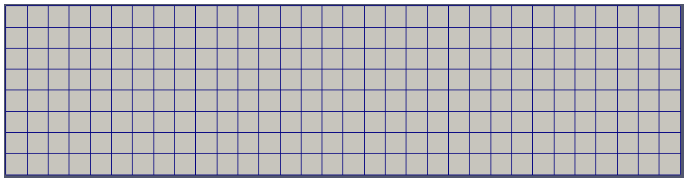

Figure 2.3: Example of a conforming rectangular mesh

We also briefly use adaptively refined meshes. Adaptive refinement refers to refining the computed solution only on specific cells estimated to have more error. The resulting meshes might not be conforming, since it is difficult to enforce that the refined mesh on a more-refined section of the mesh has no vertices in the middle of an edge on a less-refined section of the mesh. We call these vertices that are placed in the middle of another cell's edge "hanging nodes." Constraints are placed on these hanging nodes to obtain a continuous solution [22, 23]. Figure 2.4 shows an example of such a mesh:

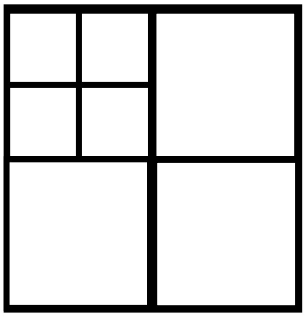

Figure 2.4: Example of an adaptively refined mesh

We express the computations on each of our cells in terms of the reference cell. Our d-dimensional reference cell is $\hat{T} = [0,1]^d$. We can then create a mapping $F_T : \hat{T} \to T$ from the reference cell to any cell T. Thus, our entire mesh can $\mathcal{T}_h$ be expressed in terms of the reference cell $\hat{T}$.

2.2.3 Polynomial spaces for each mesh cell

We next discuss the definitions of the previously-mentioned finite-dimensional spaces V^h on each cell [2]. We begin with definitions of function spaces whose functions have scalar outputs, then use these objects to construct function spaces with vector-valued functions. Throughout, we let $\mathbf{x} = (x_1, ..., x_d)$ be a d-dimensional vector.

Definition 2.2.1. *We define* $\hat{\mathbf{P}}_{\mathbf{k}}$ *as the polynomial space in the variables* $x_1, ..., x_d$ *with real coefficients and of total degree at most* k*, defined on the reference cell* $\hat{T} = [0,1]^d$ *(i.e.* $x_1, ..., x_d \in [0,1]$*). Then we have*

$$\hat{\mathbf{P}}_{\mathbf{k}} := \{f(\mathbf{x}) := \textstyle\sum_{0\leq i_1,...,i_d\leq k;\ i_1+\cdots+i_d\leq k} a_{i_1...i_d} x_1^{i_1} \cdots x_d^{i_d} : a_{i_1...i_d} \in \mathbb{R}\}.$$

Definition 2.2.2. *We define* $\hat{\mathbf{Q}}_{\mathbf{k}}$ *as the polynomial space in the variables* $x_1, ..., x_d$ *with real coefficients and of degree at most* k *in each variable, defined on the reference cell* $\hat{T} = [0,1]^d$ *(i.e.* $x_1, ..., x_d \in [0,1]$*). Then we have*

$$\hat{\mathbf{Q}}_{\mathbf{k}} = \{f(\mathbf{x}) := \textstyle\sum_{0\leq i_1,...,i_d\leq k} a_{i_1...i_d} x_1^{i_1} \cdots x_d^{i_d} : a_{i_1...i_d} \in \mathbb{R}\}.$$

We can now construct a definition for our global scalar-valued function space on our whole domain Ω by combining our scalar-valued polynomial space $\hat{\mathbf{Q}}_{\mathbf{k}}$ defined on our reference cell and our mappings F_T.

Definition 2.2.3. *Our global scalar-valued continuous polynomial space is*

$\mathbf{Q}_{\mathbf{k}} := \{v \in C(\Omega) :\ v|_T \circ F_T \in \hat{\mathbf{Q}}_{\mathbf{k}},\ \forall T \in \mathcal{T}_h\}$*, where* $C(\Omega)$ *is the space of continuous functions defined on* Ω*.*

Definition 2.2.4. *Our global scalar-valued discontinuous polynomial space is*

$\mathbf{dQ}_{\mathbf{k}} := \{v : v|_T \circ F_T \in \hat{\mathbf{Q}}_{\mathbf{k}},\ \forall T \in \mathcal{T}_h\}.$

We use one copy of the scalar space for each component of our problem. Since our displacements $\mathbf{u} : \mathbb{R}^d \to \mathbb{R}^d$, where $d = 2$ or 3, we represent each component of $\mathbf{u}$'s output with $\mathbf{Q_k}$, and denote our thus-composed overall finite element space as $\mathbf{Q_k^d} := \mathbf{Q_k} \times \cdots \times \mathbf{Q_k}$ (d copies of $\mathbf{Q_k}$).

2.2.4 Quadrature

Our proposed setup still has one more computational issue. Integrating to compute each element of the coefficient matrix A of our linear system $AU = F$ exactly is at best difficult and in most cases impossible. Instead, we approximate each of our integrals by using quadrature. In other words, the integral over a domain Ω of a function $f : \Omega \to \mathbb{R}^d$ can be approximated as follows: $\int_\Omega f \approx Q(f) := \sum_q f(\mathbf{x_q}) w_q$, where each $\mathbf{x_q} \in \Omega$ is called a "quadrature point," and each $w_q \in \mathbb{R}$ is a predetermined value called a "weight" [2].

Combining all these concepts gives us a version of A_{ij} we can actually compute [20]. In the following statements, F_T^{-1} refers to the inverse of the mapping from the reference cell $\hat{T}$ to the cell T. This inverse mapping allows us to compute quantities on the reference cell and then map them to the correct values for a given cell T. The points $\hat{\mathbf{x}}_q$ refer to quadrature points on the reference cell $\hat{T}$. The Jacobian of the inverse mapping F_T^{-1} is written J_T^{-1}, and the determinant of the Jacobian of the mapping F_T is written $\det J_T$. We denote the number of quadrature points we are using by Q. Each coefficient matrix element A_{ij} is then

$$
\begin{aligned}
A_{ij} &= \lambda \int_\Omega (\text{div } \phi_{\mathbf{i}}) \cdot (\text{div } \phi_{\mathbf{j}}) + 2\mu \int_\Omega \varepsilon(\phi_{\mathbf{i}}) : \varepsilon(\phi_{\mathbf{j}}) \\
&= \lambda \Big(\sum_{T \in \mathcal{T}_h} \int_T (\text{div } \phi_{\mathbf{i}})(\text{div } \phi_{\mathbf{j}}) \Big) + 2\mu \Big(\sum_{T \in \mathcal{T}_h} \int_T \varepsilon(\phi_{\mathbf{i}}) : \varepsilon(\phi_{\mathbf{j}}) \Big) \\
&= \lambda \Big(\sum_{T \in \mathcal{T}_h} \int_T J_T^{-1}(\hat{\mathbf{x}})(\text{div } \hat{\phi}_{\mathbf{i}}(\hat{\mathbf{x}})) J_T^{-1}(\hat{\mathbf{x}})(\text{div } \hat{\phi}_{\mathbf{j}}(\hat{\mathbf{x}})) |\text{det } J_T(\hat{\mathbf{x}})| \Big) \\
&\quad + 2\mu \Big(\sum_{T \in \mathcal{T}_h} \int_T J_T^{-1}(\hat{\mathbf{x}}) \varepsilon(\phi_{\mathbf{i}}) : J_T^{-1}(\hat{\mathbf{x}}) \varepsilon(\phi_{\mathbf{j}}) |\text{det } J_T(\hat{\mathbf{x}})| \Big) \\
&= \lambda \Big(\sum_{T \in \mathcal{T}_h} \Big(\sum_{q=1}^{Q} \Big(J_T^{-1}(\hat{\mathbf{x}}_{\mathbf{q}})(\text{div } \hat{\phi}_{\mathbf{i}}(\hat{\mathbf{x}}_{\mathbf{q}})) J_T^{-1}(\hat{\mathbf{x}}_{\mathbf{q}})(\text{div } \hat{\phi}_{\mathbf{j}}(\hat{\mathbf{x}}_{\mathbf{q}})) |\text{det } J_T(\hat{\mathbf{x}}_{\mathbf{q}})| \mathbf{w}_{\mathbf{q}} \Big) \Big) \Big) \\
&\quad + 2\mu \Big(\sum_{T \in \mathcal{T}_h} \Big(\sum_{q=1}^{Q} \Big(J_T^{-1}(\hat{\mathbf{x}}_{\mathbf{q}}) \varepsilon(\phi_{\mathbf{i}}) : J_T^{-1}(\hat{\mathbf{x}}_{\mathbf{q}}) \varepsilon(\phi_{\mathbf{j}}) |\text{det } J_T(\hat{\mathbf{x}}_{\mathbf{q}})| \mathbf{w}_{\mathbf{q}} \Big) \Big) \Big)
\end{aligned}
$$

Similarly, we compute each element of F as

$$
\begin{aligned}
F_i &= \sum_{T \in \mathcal{T}_h} \Big(\sum_{q=1}^{Q} \Big(J_T^{-1}(\hat{\mathbf{x}}_{\mathbf{q}}) \mathbf{f}(\hat{\mathbf{x}}_{\mathbf{q}}) J_T^{-1}(\hat{\mathbf{x}}_{\mathbf{q}}) \phi_{\mathbf{i}}(\hat{\mathbf{x}}_{\mathbf{q}}) |\text{det } J_T(\hat{\mathbf{x}}_{\mathbf{q}})| \mathbf{w}_{\mathbf{q}} \Big) \Big) \\
&\quad + \sum_{T|_{\partial\Omega_N} \in \mathcal{T}_h|_{\partial\Omega_N}} \Big(\sum_{q=1}^{Q} \Big(J_T^{-1}(\hat{\mathbf{x}}_{\mathbf{q}}) \mathbf{g}(\hat{\mathbf{x}}_{\mathbf{q}}) J_T^{-1}(\hat{\mathbf{x}}_{\mathbf{q}}) \phi_{\mathbf{i}}(\hat{\mathbf{x}}_{\mathbf{q}}) |\text{det } J_T(\hat{\mathbf{x}}_{\mathbf{q}})| \mathbf{w}_{\mathbf{q}} \Big) \Big)
\end{aligned}
$$

where $T|_{\partial\Omega_N}$ refers to the part of each cell that is on the boundary, and $\mathcal{T}_h|_{\partial\Omega_N} \subset \mathcal{T}_h$ refers to the cells of the mesh that are on the boundary.

Our discretized problem is then to solve the linear system $AU = F$, where each element A_{ij} of A and each element F_i of F is computed as above.

2.2.5 Well-posedness of the discretized problem

The well-posedness of the discrete problem follows from the well-posedness of our weak form and from Céa's Lemma, stated below [3].

Theorem 2.2.5. ***(Céa's Lemma.)*** *Suppose the bilinear form a is coercive with coercivity constant α and is bounded with boundedness constant C, where $0 < \alpha \leq C$ and $H_0^m(\Omega) \subset V \subset H^m(\Omega)$ and V is a Hilbert space. In addition, suppose $\mathbf{u}$ and $\mathbf{u^h}$ are the solutions of the weak form and the discretized weak form in V and $V^h \subset V$, respectively. Then*

$$\|\mathbf{u} - \mathbf{u^h}\|_m \leq \tfrac{C}{\alpha} \inf_{\mathbf{v^h} \in V^h} \|\mathbf{u} - \mathbf{v^h}\|_m.$$

Céa's Lemma gives us the best-approximation error bound for the discretized solution. Since the best-approximation error converges to 0 as $h \to 0$, we expect our discretized solution $\mathbf{u^h}$ to converge to the true solution $\mathbf{u}$ [2]; i.e., $\lim\limits_{h\to 0} \|\mathbf{u^h} - \mathbf{u}\|_{[H^1(\Omega)]^d} = 0$. Additionally, if we use an H^1-conformal finite element approximation of our problem, we have $\mathbf{u} \in [H^{\ell+1}(\Omega)]^d \cap V_{DN}$ for some $1 \leq \ell \leq k$, where k refers to the degree of our polynomial space defined above, then there exists c such that for all h, $\|\mathbf{u^h} - \mathbf{u}\|_{[H^1(\Omega)]^d} \leq ch^\ell |\mathbf{u}|_{[H^{\ell+1}(\Omega)]^d}$, where $|\cdot|_{[H^{\ell+1}(\Omega)]^d}$ refers to the $[H^{\ell+1}(\Omega)]^d$ seminorm [2]. We also have the error estimate $\|\mathbf{u} - \mathbf{u^h}\|_{[L^2(\Omega)]^d} \leq h^k \|\mathbf{u}\|_{[H^{k+1}(\Omega)]^d}$ [4].

Thus, we have a well-posed discretized system such that we expect the solution to the discretized problem to converge to the true solution as we refine our mesh.

Chapter 3

Locking of the Q_1 and Q_2 Finite Elements for Nearly Incompressible Materials

3.1 Nearly incompressible materials

We say a solid material is *incompressible* if applying pressure to it does not change its shape [24]. Thus, a nearly incompressible solid's shape does not change very much under pressure. Examples of nearly incompressible elastic materials include natural rubber [25] and solid propellants [26, 27].

Mathematically speaking, nearly incompressible materials are often characterized by Lamé's first parameter λ large or by Poisson's parameter ν close to $\frac{1}{2}$ [2, 16, 3]. Poisson's parameter ν can be expressed in terms of μ and λ with the following equation [14]: $\nu = \frac{\lambda}{2(\lambda+\mu)}$. For a fixed μ, these two characterizations of incompressibility are equivalent. We can see this by writing lambda in terms of μ and ν: $\lambda = \dfrac{2\mu\nu}{1-2\nu}$ [14]. If we fix μ and let ν approach $\frac{1}{2}$ from the left (notice that ν

cannot approach $\frac{1}{2}$ from the right given the permissible values for λ and μ), we obtain $\lim_{\nu \to \frac{1}{2}^-} \lambda = \lim_{\nu \to \frac{1}{2}^-} \dfrac{2\mu\nu}{1-2\nu} = \infty$.

3.2 What is locking?

Locking is a phenomenon that occurs in finite element approximations of the pure displacement formulation of linear elasticity for certain nearly incompressible materials [3]. According to [2], locking is inaccuracy of the displacement solution $\mathbf{u}^{\mathbf{h}}$. More specifically, locking occurs when the finite element computation produces unrealistically small displacements [3]. Locking arises for large values of λ [8], which is one of our characterizations for a nearly incompressible material. [2] provides an example of a locking phenomenon showing displacements that were smaller than they ought to be for a large value of $\frac{\lambda}{\mu}$. Every locking example in [5] demonstrates displacements that are smaller (in norm) on a coarse mesh than they should be for ν is near $\frac{1}{2}$, our other characterization for a nearly incompressible material. In Table 5 of [6], we see that certain finite elements produce overly small displacements for $\nu = 0.499$, but more reasonable displacements for $\nu = 0.3$. We can intuitively understand this phenomenon as that the model "locks", or refuses to move enough, on a coarse mesh.

3.3 Theory for locking of nearly incompressible materials

We can analyze from a mathematical perspective why locking occurs [3].

Firstly, a large λ allows large errors. Recall from our earlier boundedness and coercivity arguments that we have

$$\alpha\|\mathbf{u}\|^2_{[H^1(\Omega)]^d} \le a(\mathbf{u},\mathbf{u}) \le C\|\mathbf{u}\|^2_{[H^1(\Omega)]^d} \text{ for all } \mathbf{u} \in [H^1(\Omega)]^d$$

where $\alpha \le \mu$ and $C = 2(\lambda+\mu)$. Also recall that Céa's Lemma gives the error bound $\|\mathbf{u}-\mathbf{u^h}\|_{[H^1(\Omega)]^d} \le \frac{C}{\alpha}\inf_{\mathbf{v^h}\in V_{DN}} \|\mathbf{u}-\mathbf{v^h}\|_{[H^1(\Omega)]^d}$. This error bound is rendered ineffective for $\frac{\lambda}{\mu}$ large, since the boundedness and coercivity constants we found previously give us $\frac{C}{\alpha} \ge \frac{2(\lambda+\mu)}{\mu} = \frac{2\lambda}{\mu}+2$. Thus, mathematically speaking, inaccurate discretized solutions are unsurprising for large λ, which agrees with our various sources mentioned above. This phenomenon is sometimes referred to as "coercivity loss" [2].

Secondly, for certain finite elements and problem setups, letting λ be large forces the norm of our discretized displacement, $\|\mathbf{u^h}\|_{[H^1(\Omega)]^d}$, to be small, even though that is not necessarily what we want [3]. We know from [3] that locking occurs when $\|\text{div } \mathbf{v^h}\|_{[L^2(\Omega)]^d} \ge C^h\|\mathbf{v^h}\|_{[L^2(\Omega)]^d}$ for all $v^h \in V^h$, where C^h is a constant that depends on h. We get such an inequality for the Q_1 finite element discretization of the pure displacement linear elasticity equations on a Timoshenko beam [3] (this method is explained in more detail in Section 3.4). Since $v^h \in V^h \subset V_{DN}$, we can also apply Corollary 2.1.17 to obtain $||\varepsilon(\mathbf{v^h})||_{[L^2(\Omega)]^d} \ge c||\mathbf{v^h}||_{[H^1(\Omega)]^d}$ for all $\mathbf{v^h} \in V^h$. Then we have

$$\begin{aligned} a(\mathbf{u^h},\mathbf{u^h}) &= \lambda\int_\Omega(\text{div } \mathbf{u^h})^2 + 2\mu\int_\Omega \varepsilon(\mathbf{u^h}) : \varepsilon(\mathbf{u^h}) \\ &\ge \lambda(C^h)^2\|\mathbf{u^h}\|^2_{[H^1(\Omega)]^d} + 2\mu c\|\mathbf{u^h}\|^2_{[H^1(\Omega)]^d} \\ &= (\lambda(C^h)^2 + 2\mu c)\|\mathbf{u^h}\|^2_{[H^1(\Omega)]^d} \end{aligned}$$

where as we previously mentioned, $2\mu c \le \mu$. Then our discretized displacement is bounded, since $\|\mathbf{u^h}\|_{[H^1(\Omega)]^d} \le \frac{1}{\lambda(C^h)^2+2\mu c}\|f\| \le \frac{1}{\lambda(C^h)^2}\|\mathbf{f}\|$ [3]. As we can see from this bound, for λ large, $\|\mathbf{u^h}\|_{[H^1(\Omega)]^d}$ is forced to be small for a fixed h. However, as h gets smaller, it can begin to compensate for the large value of λ. Thus, we expect $\|\mathbf{u^h}\|_{[H^1]^d}$

to eventually rise to a reasonable value for a fixed large λ as we decrease h. In other words, for a large value of λ, we expect a discretized solution for a Timoshenko beam computed on a rectangular mesh of Q_1 elements (for example) to be too small on a coarse mesh, but more accurate on a fine mesh.

3.4 Examples of locking

In this section, we demonstrate locking on a Timoshenko beam, with both Q_1 and Q_2 elements. When we say we use a Q_k element, we mean that we solve Equation 2.1 for $\mathbf{u^h} \in \mathbf{Q_k^2}$ (note that we use dimension $d = 2$ for our experiments). We note here that we cannot model a fully incompressible material with the pure displacement formulation on Q_1 or Q_2, since then we would need $\frac{1}{2} = \nu = \frac{\lambda}{2(\lambda+\mu)}$. To achieve this we must have $\mu = 0$, which we already established is not a valid value for this parameter.

3.4.1 Problem setup

Our numerical examples of locking come from a setup discussed in [10]. We examine a beam of height 2 and length 8 which is fixed at the left edge and has a force equally applied to it at every point along its right edge (pictured in Figure 3.1). We define the y-axis to be the vertical axis and the x-axis to be the horizontal axis.

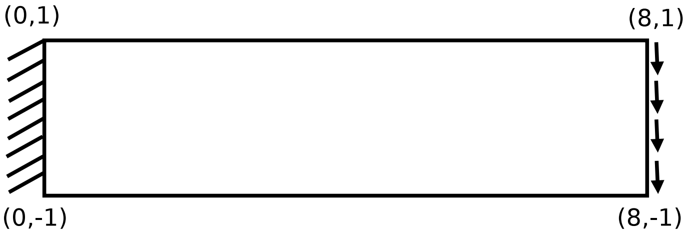

Figure 3.1: Diagram of Timoshenko beam setup.

We fix $\mu = 100$, and consider $\lambda = 100$, 5×10^4, and 5×10^5 (these values were chosen because they result in reasonable displacements for a beam 8 units long). These values for λ and μ imply ν values of 0.25, 0.499, and 0.4999, respectively (the first value is exact, and the last two values have been rounded to 5 decimal places). We thus have a "reference" case where our material is not nearly incompressible, and two nearly incompressible cases.

3.4.2 Q_1 and Q_2 Finite Elements

The dealii implementation of the Q_1 and Q_2 finite elements was used with $2k + 2$ Gaussian quadrature points in each space dimension, where k is the degree of the polynomial space. Standard Gaussian weights are used for each quadrature point of Q_1 and Q_2. The basis functions of Q_1 are linear, and the basis functions of Q_2 are quadratic. Figures 3.2 and 3.3 depict the Q_1 and Q_2 reference cells with their quadrature points.

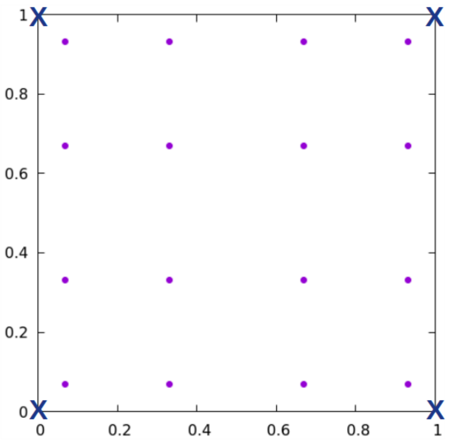

Figure 3.2: Q_1 reference cell with quadrature points $(\cdot)$ and support points (x)

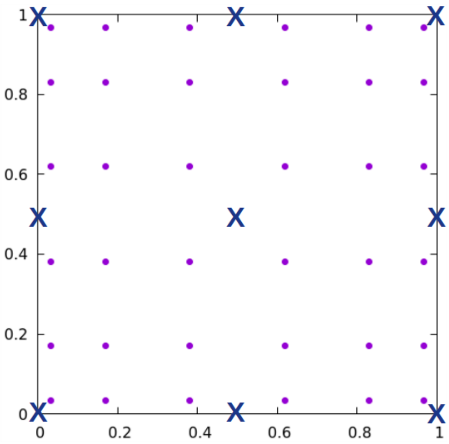

Figure 3.3: Q_2 reference cell with quadrature points $(\cdot)$ and support points (x)

Here our h is the length of the diagonal of a single (rectangular) mesh cell.

Since our mesh is subdivided into equally-size rectangular elements, h is the same for every element. Here we consider a mesh with $h = \sqrt{\frac{1}{2}} = 0.707107$ to be coarse, and a mesh with $h = \sqrt{\frac{1}{512}} = 0.0441942$ to be fine. Figures 3.4 and 3.5 depict our beam with each of these meshes.

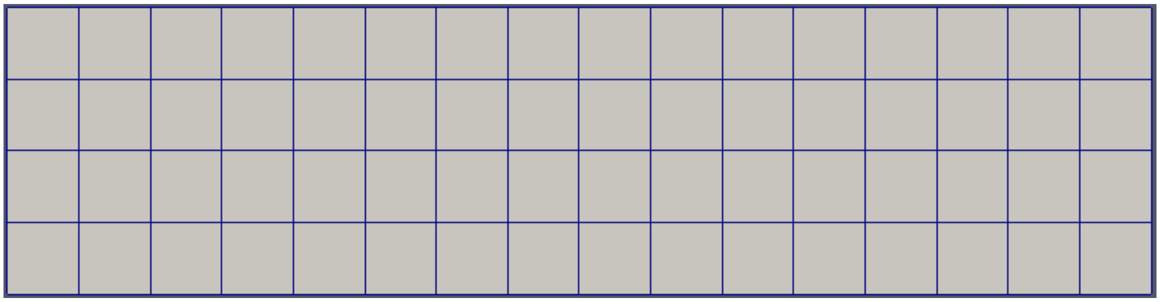

Figure 3.4: Mesh for beam with $h = 0.707107$

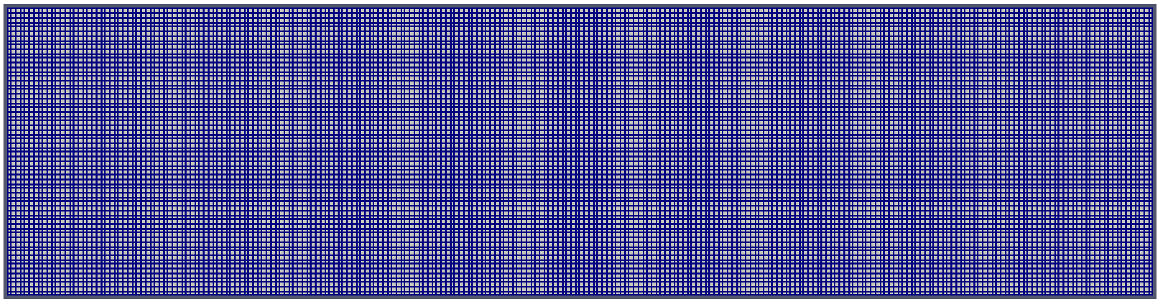

Figure 3.5: Mesh for beam with $h = 0.0441942$

We can intuitively see the locking effect with pictures of our beam model on a coarse mesh and on a fine mesh for each value of λ. The pictures were visualized in Paraview 5.4 [28]. The "Warp by Vector" filter with a scale of 1 was applied to show the displacement of the beam.

The Q_1 element exhibits severe locking.

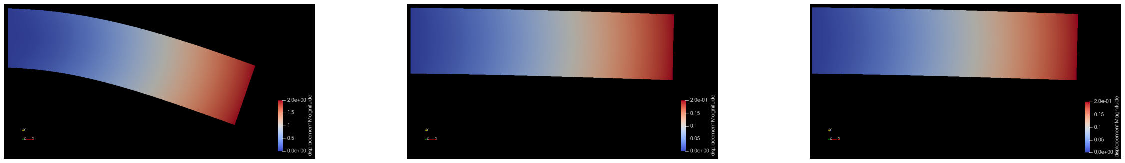

$\mu = 100, \lambda = 100$ $\mu = 100, \lambda = 5 \times 10^4$ $\mu = 100, \lambda = 5 \times 10^5$

Figure 3.6: Q_1 coarse mesh solutions.

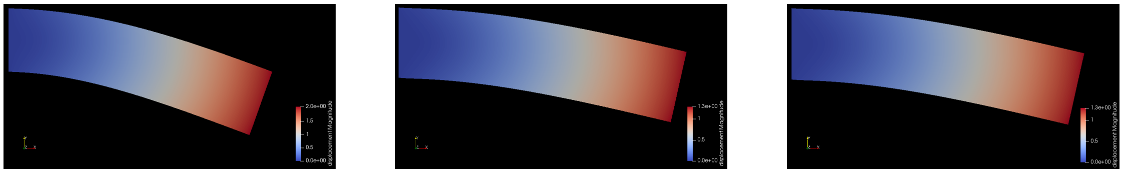

$\mu = 100, \lambda = 100$ $\mu = 100, \lambda = 5 \times 10^4$ $\mu = 100, \lambda = 5 \times 10^5$

Figure 3.7: Q_1 fine mesh solutions.

The Q_2 element's locking is more subtle. We include the visualizations for the sake of completeness, although the more precise values given in the table below are necessary to see the locking.

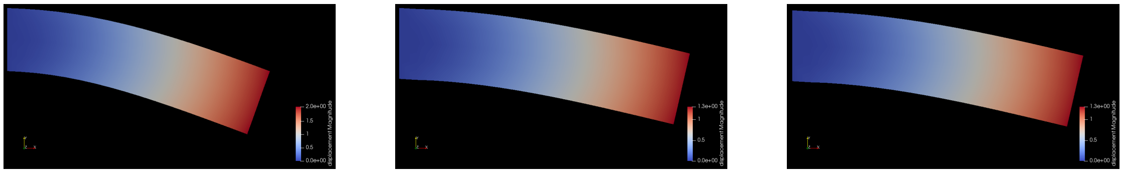

$\mu = 100, \lambda = 100$ $\mu = 100, \lambda = 5 \times 10^4$ $\mu = 100, \lambda = 5 \times 10^5$

Figure 3.8: Q_2 coarse mesh solutions.

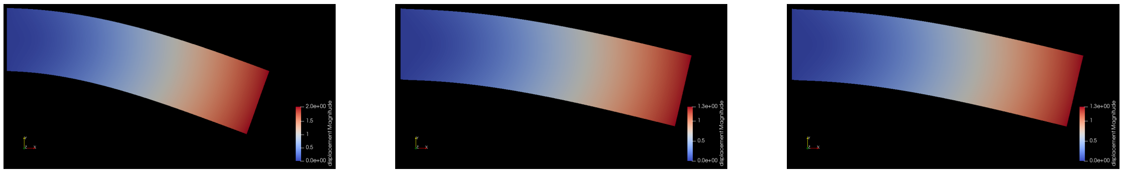

$\mu = 100, \lambda = 100$ $\mu = 100, \lambda = 5 \times 10^4$ $\mu = 100, \lambda = 5 \times 10^5$

Figure 3.9: Q_2 fine mesh solutions.

In order to examine locking more precisely, we also show a table with the y-displacements of the point $(8, -1)$ for the Q_1 and Q_2 discretizations.

	$\mathbf{Q_1}$			$\mathbf{Q_2}$		
$(\mu = 100)$	$\lambda = 100,$	$\lambda = 5 \times 10^4,$	$\lambda = 5 \times 10^5,$	$\lambda = 100,$	$\lambda = 5 \times 10^4,$	$\lambda = 5 \times 10^5,$
h	$\nu = 0.25$	$\nu = 0.499$	$\nu = 0.4999$	$\nu = 0.25$	$\nu = 0.499$	$\nu = 0.4999$
0.707107	-1.93324	-0.200963	-0.0933249	-2.00141	-1.28297	-1.27746
0.353553	-1.98402	-0.446974	-0.131043	-2.00278	-1.30861	-1.30472
0.176777	-1.99807	-0.842845	-0.259832	-2.00326	-1.31904	-1.3158
0.0883883	-2.00196	-1.14013	-0.572642	-2.00344	-1.32336	-1.3205
0.0441942	-2.00307	-1.26541	-0.962982	-2.00351	-1.32521	-1.32254
Extrapolated	-2.00357	-1.32685	-1.32437	-2.00357	-1.32685	-1.32437
Relative difference	0.03510	0.84854	0.92953	0.00108	0.03307	0.03542

Table 3.1: Locking: Q_1 and Q_2 y-displacements of the point $(8, -1)$

Simply comparing the coarse- and fine-mesh displacements in the incompressible cases demonstrates the locking we previously mentioned. The coarse-mesh displacements for Q_1 are dramatically smaller than those on the fine mesh, which is precisely the locking effect we described. This effect can also be seen for the Q_2 displacements, although it is less drastic. For a material that is certainly not nearly incompressible ($\lambda = 100$ or $\nu = 0.25$), however, the difference between the coarse-mesh and fine-mesh solutions is much smaller.

We also calculate for comparison the relative difference between the coarse-mesh solutions and extrapolated solutions. The extrapolated solutions were determined using Richardson extrapolation with the last three Q_2 displacements for each value of λ, since Q_2 discretization is more accurate than Q_1 discretization. Specifically, we created our extrapolation using the following derivation.

Using a Taylor series expansion, we get that our real solution

$A^* = A(h) - c_1 h - c_2 h^2 + O(h^3)$, where $A(h)$ is our approximation for a given mesh refinement defined by h, and $c_1, c_2 \in \mathbb{R}$ are constants. Then

$A(h) = A^* + c_1 h + c_2 h^2 + O(h^3)$. Note that plugging in $\frac{h}{2}$ and $\frac{h}{4}$ gives us

$$A(\tfrac{h}{2}) = A^* + c_1\tfrac{h}{2} + c_2\tfrac{h^2}{4} + O(\tfrac{h^3}{8}) = A^* + c_1\tfrac{h}{2} + c_2\tfrac{h^2}{4} + O(h^3) \text{ and}$$

$$A(\tfrac{h}{4}) = A^* + c_1\tfrac{h}{4} + c_2\tfrac{h^2}{16} + O(\tfrac{h^3}{64}) = A^* + c_1\tfrac{h}{4} + c_2\tfrac{h^2}{16} + O(h^3).$$

We define

$$B(\tfrac{h}{2}) := 2A(\tfrac{h}{2}) - A(h) = A^* - c_2\tfrac{h^2}{2} + O(\tfrac{3h^3}{4}) = A^* - c_2\tfrac{h^2}{2} + O(h^3) \text{ and}$$

$$B(\tfrac{h}{4}) := 2A(\tfrac{h}{4}) - A(\tfrac{h}{2}) = A^* - c_2\tfrac{h^2}{8} + O(h^3).$$

We then have the Richardson extrapolation

$$\begin{aligned} R(h) &= \frac{4B(\frac{h}{4}) - B(\frac{h}{2})}{3} = \frac{4A^* - c_2\frac{h^2}{2} + O(h^3) - A^* + c_2\frac{h^2}{2} + O(h^3)}{3} \\ &= \frac{3A^* + O(h^3)}{3} = A^* + O(h^3) \end{aligned}$$

So the approximation we use for our exact solution is

$$A^* \approx \frac{4B(\frac{h}{4}) - B(\frac{h}{2})}{3} = \frac{8A(\frac{h}{4}) - 6A(\frac{h}{2}) + A(h)}{3}$$

Note that for $\lambda = 100$ ($\nu = 0.25$), the relative difference for Q_1 is on the order of 10^{-2}, whereas in the nearly incompressible cases this difference jumps to nearly 1. For Q_2 we note a relative difference on the order of 10^{-3} for the $\lambda = 100$ ($\nu = 0.25$) case, which rises to the order of 10^{-2} for the nearly incompressible cases. These calculations show locking in a way agnostic to the magnitude of the correct value of the displacement, which varies somewhat with the parameter values.

Chapter 4

Methods

In this chapter we introduce several non-standard methods in the hopes that some of them solve locking. Reduced integration and displacement-pressure formulation methods are considered.

4.1 Selective under-integration

One strategy that has been explored to remedy this locking phenomenon is to reduce the number of quadrature points used to approximate the term $\lambda \int_\Omega (\text{div } \mathbf{u})(\text{div } \mathbf{v})$ [19, 7, 8, 5]. Intuitively, the goal is to lessen the effect λ has on our weak form, and thus lessen the previously-discussed reductive effect it has on $\|\mathbf{u}^\mathbf{h}\|_{[H^1(\Omega)]^d}$ for certain finite elements. With this strategy each element of our coefficient matrix A is

$$\begin{aligned} A_{ij} = \lambda\Big(\sum_{T \in \mathcal{T}_h} \Big(\sum_{q=1}^{Q_0} \Big(J_T^{-1}(\hat{\mathbf{x}}_\mathbf{q})(\text{div } \hat{\phi}_\mathbf{i}(\hat{\mathbf{x}}_\mathbf{q})) J_T^{-1}(\hat{\mathbf{x}}_\mathbf{q})(\text{div } \hat{\phi}_\mathbf{j}(\hat{\mathbf{x}}_\mathbf{q})) |\text{det } J_T(\hat{\mathbf{x}}_\mathbf{q})| \mathbf{w}_\mathbf{q} \Big)\Big)\Big) \\ + 2\mu\Big(\sum_{T \in \mathcal{T}_h} \Big(\sum_{q=1}^{Q} \Big(J_T^{-1}(\hat{\mathbf{x}}_\mathbf{q}) \varepsilon(\phi_\mathbf{i}) : J_T^{-1}(\hat{\mathbf{x}}_\mathbf{q}) \varepsilon(\phi_\mathbf{j}) |\text{det } J_T(\hat{\mathbf{x}}_\mathbf{q})| \mathbf{w}_\mathbf{q} \Big)\Big)\Big) \end{aligned}$$

where Q_0 denotes the number of quadrature points used to approximate $\lambda \int_\Omega (\text{div } \mathbf{u})(\text{div } \mathbf{v})$

and $Q_0 < Q$. We next introduce some reduced-integration elements.

4.1.1 Q_1-midpoint

We use the deal.II implementation of the Q_1 finite element for this strategy. Four-point Gaussian quadrature (in both space dimensions) was used on the term $2\mu \int_\Omega \varepsilon(\mathbf{u}) : \varepsilon(\mathbf{v})$, and the deal.II midpoint quadrature (QMidpoint$\langle$dim$\rangle$) (in both space dimensions) was used on the term $\lambda \int_\Omega (\text{div } \mathbf{u})(\text{div } \mathbf{v})$. Thus, we did not force the boundary values of adjacent mesh cells to agree on the value of the $\lambda \int_\Omega (\text{div } \mathbf{u})(\text{div } \mathbf{v})$ term. The weight given to the single quadrature point of the midpoint quadrature is, of course, 1. The reference cell of this element is pictured in Figure 4.1.

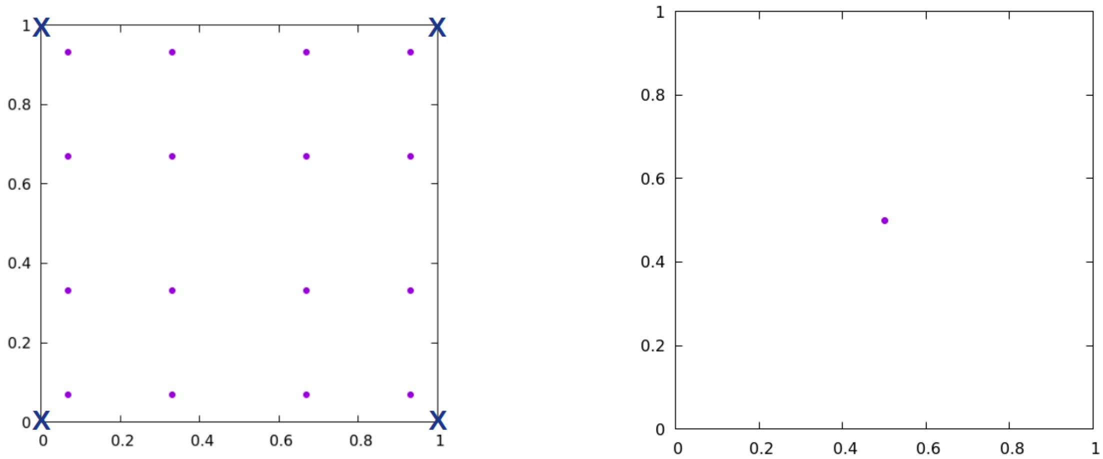

Quadrature for $2\mu \int_\Omega \varepsilon(\mathbf{u}) : \varepsilon(\mathbf{v})$

Quadrature for $\lambda \int_\Omega (\text{div } \mathbf{u})(\text{div } \mathbf{v})$

Figure 4.1: Q_1-midpoint reference element with quadrature points

[7] assures us that this element cures locking.

4.1.2 Q_2-gauss2

We next examine the Q_2-gauss2 finite element. Six-point Gaussian quadrature (in both space dimensions) was used on the term $2\mu \int_\Omega \varepsilon(\mathbf{u}) : \varepsilon(\mathbf{v})$, and 2-point

Gaussian quadrature (QGauss⟨dim⟩ (2))(in both space dimensions) was used on the term $\lambda \int_\Omega (\text{div } \mathbf{u})(\text{div } \mathbf{v})$. The weight given to each quadrature point of the 2-point Gaussian quadrature is 0.25. The reference cell of this element is pictured in Figure 4.2.

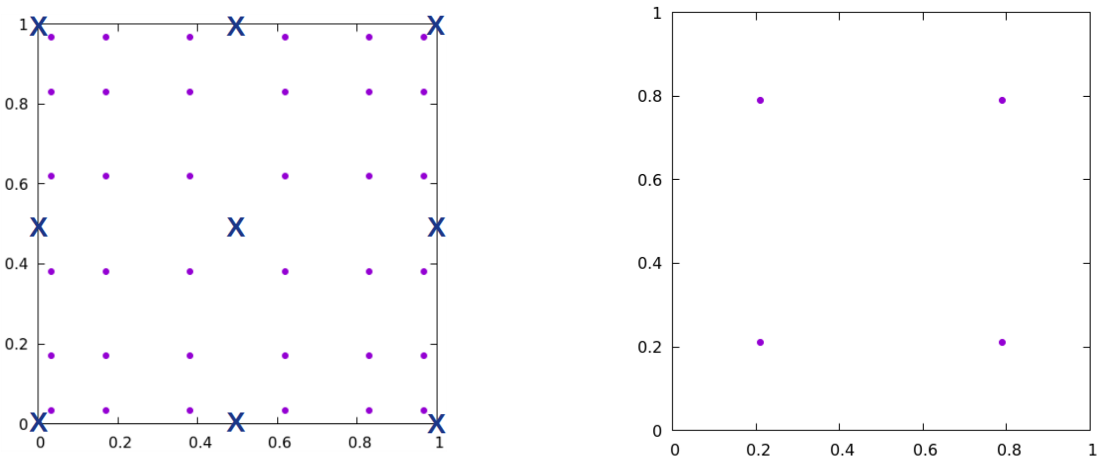

Quadrature for $2\mu \int_\Omega \varepsilon(\mathbf{u}) : \varepsilon(\mathbf{v})$

Quadrature for $\lambda \int_\Omega (\text{div } \mathbf{u})(\text{div } \mathbf{v})$

Figure 4.2: Q_2−gauss2 reference element with quadrature points

[7] tells us that this element also solves locking, and additionally gives an example where it produces an accurate solution.

4.2 Displacement-pressure formulation

In this setup we use the displacement-pressure formulation of the linear elasticity questions introduced in Chapter 2.

4.2.1 $Q_1 - dGP_0$

We discretize with the finite element $Q_1 - dGP_0$ as implemented in deal.II (i.e., FESystem⟨dim⟩(FE_Q⟨dim⟩(1), dim, FE_DGP⟨dim⟩(0), 1)). The quadrature for this element is the same as that for the Q_1 element. When we say we use the $Q_k - dGP_{k-1}$ element, we mean that we solve Equation 2.2 for $\mathbf{u^h} \in \mathbf{Q_k^2}$ and $p^h \in \mathbf{dGP_{k-1}^2}$.

By [4], we have the error estimates $\|\nabla(\mathbf{u} - \mathbf{u^h})\|_{[L^2(\Omega)]^d} \leq C_1 h \|\mathbf{f}\|_{[L^2(\Omega)]^d}$ and $\|\mathbf{u} - \mathbf{u^h}\|_{[L^2(\Omega)]^d} \leq C_2 h^2 \|\mathbf{f}\|_{[L^2(\Omega)]^d}$, where neither C_1 nor C_2 depend on h or λ. We can combine these estimates using the triangle inequality to obtain

$$\begin{aligned}
\|\mathbf{u} - \mathbf{u^h}\|_{[H^1(\Omega)]^d} &\leq \|\mathbf{u} - \mathbf{u^h}\|_{[L^2(\Omega)]^d} + \|\nabla(\mathbf{u} - \mathbf{u^h})\|_{[L^2(\Omega)]^d} \\
&\leq C_1 h^2 \|\mathbf{f}\|_{[L^2(\Omega)]^d} + C_2 h \|\mathbf{f}\|_{[L^2(\Omega)]^d} \\
&< C_1 h \|\mathbf{f}\|_{[L^2(\Omega)]^d} + C_2 h \|\mathbf{f}\|_{[L^2(\Omega)]^d} \\
&\leq \max\{C_1, C_2\} h \|\mathbf{f}\|_{[L^2(\Omega)]^d}
\end{aligned}$$

Thus we have an $[H^1(\Omega)]^d$ error estimate not depending on λ for this method.

4.2.2 $Q_2 - dGP_1$

We discretize with the finite element $Q_2 - dGP_1$ as implemented in deal.II (i.e., FESystem⟨dim⟩(FE_Q⟨dim⟩(2), dim, FE_DGP⟨dim⟩(1), 1)). The quadrature for this element is the same as that for the Q_2 element. [8] gives us stability of this element.

4.3 Equivalence

It is sometimes, but not always, possible to establish an equivalence between a reduced integration method and a displacement-pressure method.

4.3.1 Equivalence of $Q_1 - dGP_0$ and Q_1-midpoint

According to [8], the $Q_1 - dGP_0$ finite element and the Q_1-midpoint reduced integration are equivalent on rectangles. We verify this numerically with the example in Table 4.1. We use the same beam setup as we did for locking.

	$\mathbf{Q_1-}$**midpoint**			$\mathbf{Q_1 - dGP_0}$		
$(\mu = 100)$	$\lambda = 100$	$\lambda = 5 \times 10^4$	$\lambda = 5 \times 10^5$	$\lambda = 100$	$\lambda = 5 \times 10^4$	$\lambda = 5 \times 10^5$
h	$\nu = 0.25$	$\nu = 0.499$	$\nu = 0.4999$	$\nu = 0.25$	$\nu = 0.499$	$\nu = 0.4999$
0.707107	-1.97755	-1.31344	-1.31082	-1.97755	-1.31344	-1.31082
0.353553	-1.99575	-1.31774	-1.31515	-1.99575	-1.31774	-1.31515
0.176777	-2.00113	-1.32197	-1.31941	-2.00113	-1.32197	-1.31941
0.0883883	-2.00277	-1.32439	-1.32185	-2.00277	-1.32439	-1.32185
0.0441942	-2.00329	-1.32561	-1.32308	-2.00329	-1.32561	-1.32308

Table 4.1: Q_1-midpoint and $Q_1 - dGP_0$ solutions for the y-displacement of the point $(8, -1)$ on our Timoshenko beam.

Notice that the y-displacements of the point $(8, -1)$ computed with the method Q_1-midpoint are exactly the same as those computed with the method $Q_1 - dGP_0$.

4.3.2 $Q_2 - dGP_1$ and Q_2-gauss2 not equivalent

The Q_2-gauss2 and $Q_2 - dGP_1$ methods produce very similar but not equivalent solutions (see Table 4.2).

	$\mathbf{Q_2}$−gauss2			$\mathbf{Q_2 - dGP_1}$		
$(\mu = 100)$	$\lambda = 100$	$\lambda = 5 \times 10^4$	$\lambda = 5 \times 10^5$	$\lambda = 100$	$\lambda = 5 \times 10^4$	$\lambda = 5 \times 10^5$
h	$\nu = 0.25$	$\nu = 0.499$	$\nu = 0.4999$	$\nu = 0.25$	$\nu = 0.499$	$\nu = 0.4999$
0.707107	-2.00172	-1.31763	-1.31505	-2.0019	-1.32095	-1.31841
0.353553	-2.00289	-1.32291	-1.32035	-2.00295	-1.32428	-1.32175
0.176777	-2.0033	-1.32503	-1.32248	-2.00332	-1.32561	-1.32307
0.0883883	-2.00346	-1.32594	-1.32341	-2.00346	-1.3262	-1.32367
0.0441942	-2.00351	-1.32635	-1.32382	-2.00352	-1.32646	-1.32393

Table 4.2: Q_2−gauss2 and $Q_2 - dGP_1$ solutions for the y-displacement of the point $(8, -1)$ on our Timoshenko beam.

Chapter 5

Results

We based our code on programs from the open-source finite element library deal.II [29, 30]. Our work extends the step-8 tutorial program [9]. It additionally uses parameter value output functionality from the step-29 tutorial program [31], mixed-boundary conditions from the step-7 tutorial program [32], and the displacement-pressure structure from the step-22 tutorial program [33]. In all cases, we solve our linear system with a direct solver, namely the SparseDirectUMFPack solver which uses UMFPACK [34]. Our code is publicly available at on Github at the link in Appendix A.

In this chapter we firstly verify that each of our methods has optimal convergence errors with a manufactured solution. We secondly verify that our methods produce the same results as those of a Timoshenko beam benchmark in [10]. Thirdly, we demonstrate that our non-standard methods cure the locking exhibited by the standard Q_1 and Q_2 elements.

5.1 Manufactured solution

The goal of using a manufactured solution is to solve the implied equation with a chosen finite element setup, and then compare that result with the actual solution. We can then judge how accurate our finite element solutions are.

5.1.1 Solution

The manufactured solution we use here is $\mathbf{u} = 0.01 \left(\begin{smallmatrix} \sin(\pi x) \\ -\pi y \cos(\pi x) \end{smallmatrix} \right)$. Notice that $\text{div } \mathbf{u} = 0.01(\pi \cos(\pi x) - \pi \cos(\pi x)) = 0$, so our manufactured solution is "divergence-free." (Remark: We ensure this, because if we had $(\text{div } \mathbf{u}) \neq 0$, then $\lambda \int_\Omega (\text{div } \mathbf{u})(\text{div } \mathbf{v})$ would almost certainly not be 0, and so we would have

$F(\mathbf{v}) = \lambda \int_\Omega (\text{div } \mathbf{u})(\text{div } \mathbf{v}) + 2\mu \int_\Omega \varepsilon(\mathbf{u}) : \varepsilon(\mathbf{v}) \to \infty$ as $\lambda \to \infty$.

Then $F(\mathbf{v})$ would not be bounded, and so we would not be able to apply the Lax-Milgram theorem to ensure a unique solution to our weak form.)

We solve our pure displacement formulation on a rectangular mesh on the domain $\Omega = [-1, 1] \times [-1, 1]$ (a fine mesh is pictured in Figure 5.1). We apply Dirichlet conditions using our manufactured solution $\mathbf{u}$ on the whole boundary.

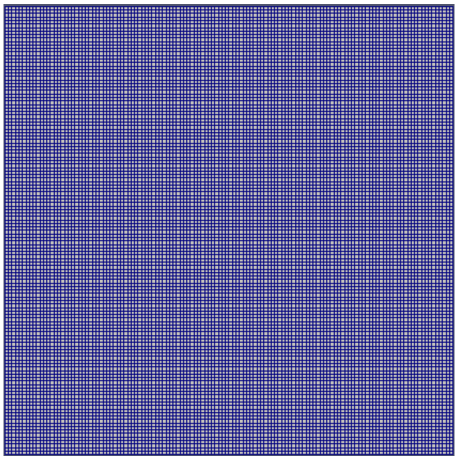

Figure 5.1: Fine mesh ($h = 0.0220971$, or 8 refinement levels) for manufactured solution

5.1.2 Calculating error rates with a manufactured solution

We base our error rate calculations on the error estimates from Chapter 1. We call the exponent on h in these estimates the "error rate" of the method. By making the assumptions that $\|\mathbf{u}-\mathbf{u^h}\|_{[L^2(\Omega)]^d} \approx ch^{k+1}$ and that c is approximately the same regardless of the value of h, we can calculate the $[L^2(\Omega)]^d$ convergence rate $k+1$. With two different h values h_1 and h_2 we can use the $[L^2(\Omega)]^d$ errors to get

$$k+1 = \ln\left(\frac{\|\mathbf{u}-\mathbf{u^{h_2}}\|_{[L^2(\Omega)]^d}}{\|\mathbf{u}-\mathbf{u^{h_1}}\|_{[L^2(\Omega)]^d}}\right) / \ln\left(\frac{h_2}{h_1}\right)$$

Similarly, we can use the $[H^1(\Omega)]^d$ errors to calculate the $[H^1(\Omega)]^d$ convergence rate

$$k = \ln\left(\frac{\|\mathbf{u}-\mathbf{u^{h_2}}\|_{[H^1(\Omega)]^d}}{\|\mathbf{u}-\mathbf{u^{h_1}}\|_{[H^1(\Omega)]^d}}\right) / \ln\left(\frac{h_2}{h_1}\right)$$

Thus, we can check whether the implementations of our finite elements produce the convergence rates we expect.

5.1.3 Standard finite elements on pure displacement formulation

5.1.3.1 Q_1 manufactured solution results

We expect $[L^2(\Omega)]^d$ convergence rates of 2 and $[H^1(\Omega)]^d$ convergence rates of 1 for the Q_1 element. Table 5.1 demonstrates these convergence rates, for both the reference case and the nearly incompressible cases. The table also shows reasonable errors in both the $[L^2(\Omega)]^d$ and $[H^1(\Omega)]^d$ norms. We see no locking in this table because we force the whole boundary to be the correct value by using Dirichlet conditions.

$\mathbf{Q_1}$ $(\mu = 1)$	h	$[L^2(\Omega)]^d$ errors	$[L^2(\Omega)]^d$ rates	$[H^1(\Omega)]^d$ errors	$[H^1(\Omega)]^d$ rates
$\lambda = 1,$	0.0883883	0.000118		0.005217	
$\nu = 0.25$	0.0441942	2.96E-05	1.998484	0.002608	1.000259
	0.0220971	7.40E-06	1.999623	0.001304	1.000061
$\lambda = 500,$	0.0883883	0.000136		0.005220	
$\nu = 0.499$	0.0441942	3.39E-05	2.001612	0.002608	1.000864
	0.0220971	8.47E-06	2.001418	0.001304	1.000216
$\lambda = 5 \times 10^4,$	0.0883883	0.000137		0.005220	
$\nu = 0.49999$	0.0441942	3.42E-05	1.997598	0.002608	1.000878
	0.0220971	8.55E-06	2.000539	0.001304	1.000227

Table 5.1: Q_1 errors and convergence rates for manufactured solution.

In Figure 5.2 we also picture the fine-mesh ($h = 0.0220971$) displacements for $\mu = 1$, with λ taking on the values $1, 500$, and 5×10^4 (the same parameter values as in our convergence table).

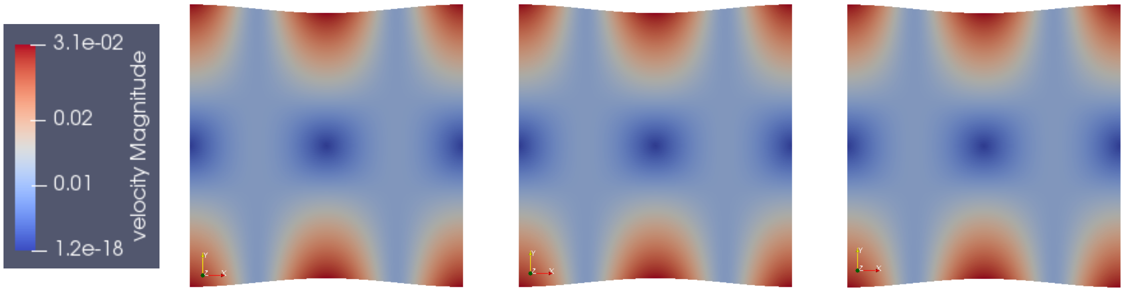

scale

$\mu = 1, \lambda = 1$

$\mu = 1, \lambda = 500$

$\mu = 1, \lambda = 5 \times 10^4$

Figure 5.2: Visualized Q_1 displacements

5.1.3.2 Q_2 manufactured solution results

We expect $[L^2(\Omega)]^d$ convergence rates of 3 and $[H^1(\Omega)]^d$ convergence rates of 2 from this element. Table 5.2 demonstrates these convergence rates and reasonable errors, for both the reference case and the nearly incompressible cases. As with Q_1, our Dirichlet conditions ensure that we see no locking.

$\mathbf{Q_2}$ $(\mu = 1)$	h	$[L^2(\Omega)]^d$ errors	$[L^2(\Omega)]^d$ rates	$[H^1(\Omega)]^d$ errors	$[H^1(\Omega)]^d$ rates
$\lambda = 1$,	0.0883883	1.27E-06		0.000132	
$\nu = 0.25$	0.0441942	1.59E-07	2.999174	3.31E-05	1.999613
	0.0220971	1.99E-08	2.999785	8.26E-06	1.999901
$\lambda = 500$,	0.0883883	1.27E-06		0.000132	
$\nu = 0.499$	0.0441942	1.59E-07	2.999586	3.31E-05	1.999661
	0.0220971	1.99E-08	2.999871	8.26E-06	1.999915
$\lambda = 5 \times 10^4$,	0.0883883	1.27E-06		0.000132	
$\nu = 0.49999$	0.0441942	1.59E-07	2.999776	3.31E-05	1.999678
	0.0220971	1.99E-08	2.999931	8.26E-06	1.999918

Table 5.2: Q_2 errors and convergence rates for manufactured solution.

In Figure 5.3, we also picture the fine-mesh ($h = 0.0220971$) displacements for $\mu = 1$, with λ taking the values $1, 500$, and 5×10^4 (the same parameter values as in our convergence table).

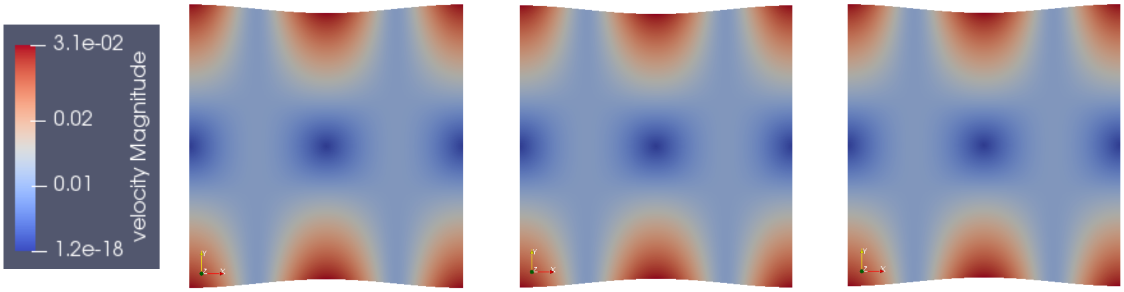

scale

$\mu = 1, \lambda = 1$

$\mu = 1, \lambda = 500$

$\mu = 1, \lambda = 5 \times 10^4$

Figure 5.3: Visualized Q_2 displacements

5.1.4 Reduced integration on pure displacement formulation

5.1.4.1 Q_1-midpoint manufactured solution results

We can see from Table 5.3 that the errors and convergence rates of this method are almost identical to those of the Q_1. Thus, despite reducing the number of quadrature points on the term $\lambda \int_\Omega (\text{div }\mathbf{u})(\text{div }\mathbf{v})$, we achieve the same accuracy and convergence, both for the reference case and the nearly incompressible cases.

$\mathbf{Q_1}$**−midpoint** ($\mu = 1$)	h	$[L^2(\Omega)]^d$ errors	$[L^2(\Omega)]^d$ rates	$[H^1(\Omega)]^d$ errors	$[H^1(\Omega)]^d$ rates
$\lambda = 1$,	0.0883883	0.000118		0.005217	
$\nu = 0.25$	0.0441942	2.96E-05	1.998562	0.002608	1.000259
	0.0220971	7.40E-06	1.999636	0.001304	1.000061
$\lambda = 500$,	0.0883883	0.000135		0.005220	
$\nu = 0.499$	0.0441942	3.39E-05	1.998473	0.002608	1.000864
	0.0220971	8.47E-06	1.999616	0.001304	1.000216
$\lambda = 5 \times 10^4$,	0.0883883	0.0001355		0.005220	
$\nu = 0.49999$	0.0441942	3.39E-05	1.998485	0.002608	1.000870
	0.0220971	8.48E-06	1.999620	0.001304	1.000221

Table 5.3: Q_1−midpoint errors and convergence rates for manufactured solution.

We also show the fine-mesh displacements for this method in Figure 5.4. Notice that they look exactly the same as those produced by using Q_1.

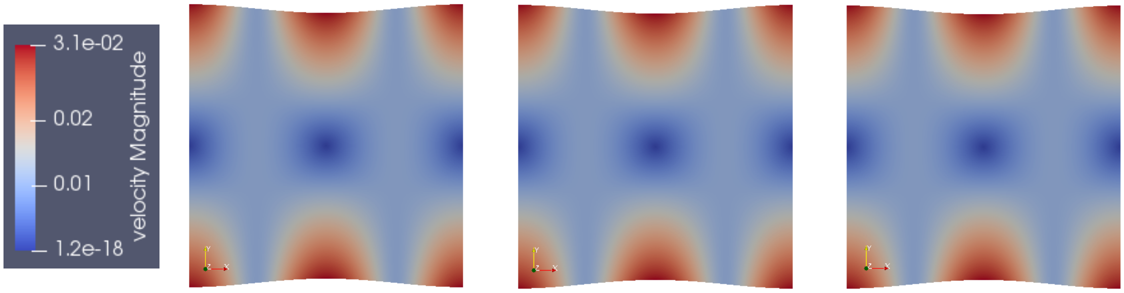

scale

$\mu = 1, \lambda = 1$ $\mu = 1, \lambda = 500$ $\mu = 1, \lambda = 5 \times 10^4$

Figure 5.4: Visualized Q_1-midpoint displacements

5.1.4.2 Q_2-gauss2 manufactured solution results

This reduced quadrature scheme gives us errors and convergence rates nearly identical to those of the Q_2 element. Thus, despite reducing the number of quadrature points on the term $\lambda \int_\Omega (\text{div } \mathbf{u})(\text{div } \mathbf{v})$, we once again achieve the same accuracy and convergence, both for the reference case and the nearly incompressible cases.

$\mathbf{Q_2}-$**gauss2** $(\mu = 1)$	h	$[L^2(\Omega)]^d$ errors	$[L^2(\Omega)]^d$ rates	$[H^1(\Omega)]^d$ errors	$[H^1(\Omega)]^d$ rates
$\lambda = 1$,	0.0883883	1.27E-06		0.000132	
$\nu = 0.25$	0.0441942	1.59E-07	2.999163	3.31E-05	1.999613
	0.0220971	1.99E-08	2.999785	8.26E-06	1.999901
$\lambda = 500$,	0.0883883	1.27E-06		0.000132	
$\nu = 0.499$	0.0441942	1.59E-07	2.999419	3.31E-05	1.999671
	0.0220971	1.99E-08	2.999842	8.26E-06	1.999914
$\lambda = 5 \times 10^4$,	0.0883883	1.27E-06		0.000132	
$\nu = 0.49999$	0.0441942	1.59E-07	2.999421	3.31E-05	1.999685
	0.0220971	1.99E-08	2.999844	8.26E-06	1.999922

Table 5.4: Q_2-gauss2 errors and convergence rates for manufactured solution.

We also note that the visualizations produced by Q_2-gauss2 (Figure 5.5) are identical to those produced by Q_2.

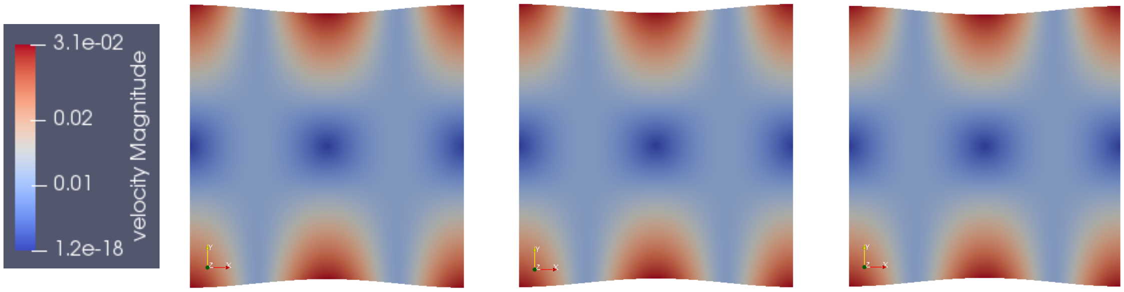

scale

$\mu = 1, \lambda = 1$

$\mu = 1, \lambda = 500$

$\mu = 1, \lambda = 5 \times 10^4$

Figure 5.5: Visualized Q_2-gauss2 displacements

5.1.5 Displacement-pressure formulation

5.1.5.1 $Q_1 - dGP_0$ displacement-pressure manufactured solution results

$Q_1 - dGP_0$ is one of the finite elements used for the Stokes' problem, and no unifying theory about its performance exists [8]. Thus, we hope for error rates similar to those of Q_1, and indeed we are not disappointed (see Table 5.5).

$\mathbf{Q_1 - dGP_0}$ $(\mu = 1)$	h	$[L^2(\Omega)]^d$ errors	$[L^2(\Omega)]^d$ rates	$[H^1(\Omega)]^d$ errors	$[H^1(\Omega)]^d$ rates
$\lambda = 1$,	0.0883883	0.000135		0.005218	
$\nu = 0.25$	0.0441942	3.38E-05	1.998903	0.002608	1.000345
	0.0220971	8.45E-06	1.999724	0.001304	1.000089
$\lambda = 500$,	0.0883883	0.000323		0.005228	
$\nu = 0.499$	0.0441942	7.90E-05	2.033950	0.002609	1.002603
	0.0220971	1.96E-05	2.012841	0.001304	1.000625
$\lambda = 5 \times 10^4$,	0.0883883	0.000333		0.005229	
$\nu = 0.49999$	0.0441942	8.21E-05	2.019246	0.002610	1.002719
	0.0220971	2.04E-05	2.011610	0.001304	1.000669

Table 5.5: $Q_1 - dGP_0$ errors and convergence rates for manufactured solution.

This method also produces visualizations that appear identical to those from our other methods (see Figure 5.6).

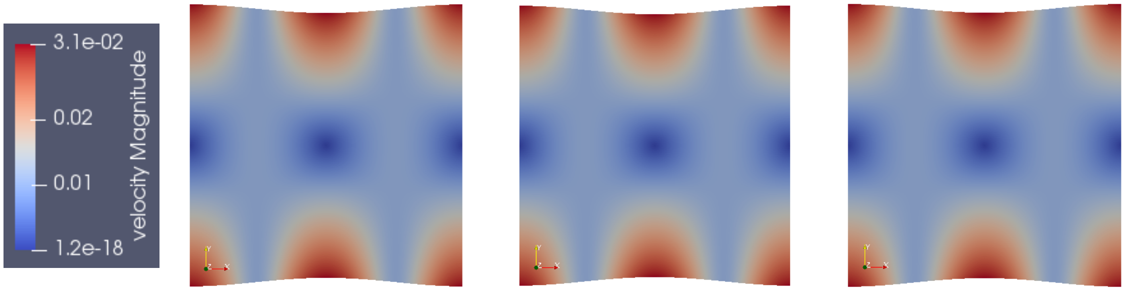

scale

$\mu = 1, \lambda = 1$

$\mu = 1, \lambda = 500$

$\mu = 1, \lambda = 5 \times 10^4$

Figure 5.6: Visualized $Q_1 - dGP_0$ displacements

5.1.6 $Q_2 - dGP_1$ displacement-pressure manufactured solution results

$Q_2 - dGP_1$ is one of the stable finite elements used for the Stokes' problem [8]. We get error rates similar to those of Q_2 (see Table 5.6).

$\mathbf{Q_2 - dGP_1}$ $(\mu = 1)$	h	$[L^2(\Omega)]^d$ errors	$[L^2(\Omega)]^d$ rates	$[H^1(\Omega)]^d$ errors	$[H^1(\Omega)]^d$ rates
$\lambda = 1$, $\nu = 0.25$	0.0883883	1.27E-06		0.000132	
	0.0441942	1.59E-07	2.999179	3.31E-05	1.999595
	0.0220971	1.99E-08	2.999795	8.26E-06	1.999897
$\lambda = 500$, $\nu = 0.499$	0.0883883	1.28E-06		0.000132	
	0.0441942	1.59E-07	3.001015	3.31E-05	1.999595
	0.0220971	1.99E-08	3.000539	8.26E-06	1.999897
$\lambda = 5 \times 10^4$, $\nu = 0.49999$	0.0883883	1.28E-06		0.000132	
	0.0441942	1.59E-07	3.001045	3.31E-05	1.999595
	0.0220971	1.99E-08	3.000559	8.26E-06	1.999897

Table 5.6: Visualized $Q_2 - dGP_1$ displacements

The visualizations from this method are once again the same (see Figure 5.7).

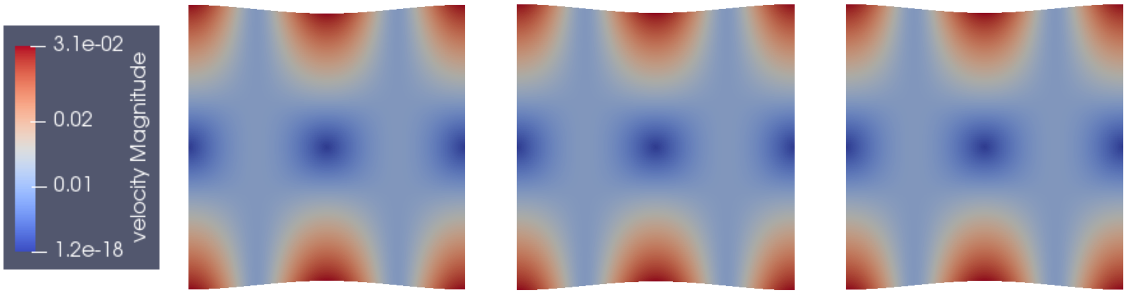

scale

$\mu = 1, \lambda = 1$

$\mu = 1, \lambda = 500$

$\mu = 1, \lambda = 5 \times 10^4$

Figure 5.7: Visualized $Q_2 - dGP_1$ displacements

5.2 Timoshenko benchmark

The authors of [10] examine the Timoshenko beam setup described already in Chapter 3. They set $\lambda = \mu = 400$ and provide plots of the discretized displacement and stress tensor elements σ_{11}, σ_{12}, and $\sigma_{12} = \sigma_{21}$ (note that $\sigma(\mathbf{u})$ is symmetric) over the left edge of the beam. The edge of the beam between the points $(0, -1)$ and $(0, 1)$ becomes the x-axis in the plots. We provide our versions of these plots and invite the reader to compare our plots to those in [10] as a second benchmark for each of our methods. We note here that the extreme stress values at the edges of our plots are consistent with [10]'s statement that the shear stress solution is singular at the left corners.

5.2.1 Global refinement solutions

We present the plots we obtained with global refinement for each of our methods in Figure 5.8. We refined our starting mesh 8 times, resulting in $h = 0.0220971$, and solved for 132354 unknowns for Q_1 and Q_1-midpoint, 526850 unknowns for Q_2 and Q_2-gauss2, 197890 unknowns for $Q_1 - dGP_0$, and 723458 unknowns for $Q_2 - dGP_1$.

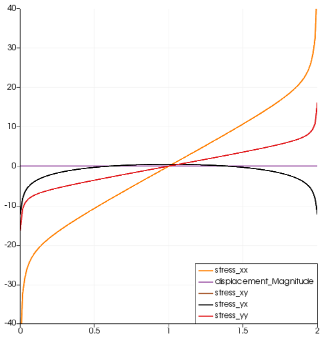

Q_1

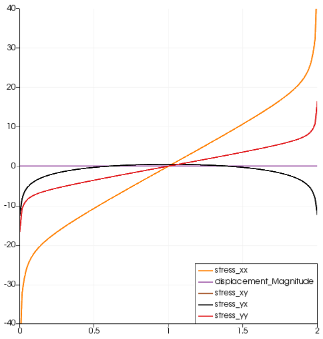

Q_1-midpoint

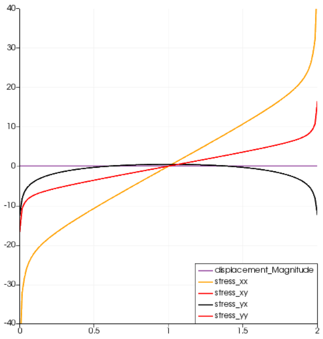

$Q_1 - dGP_0$

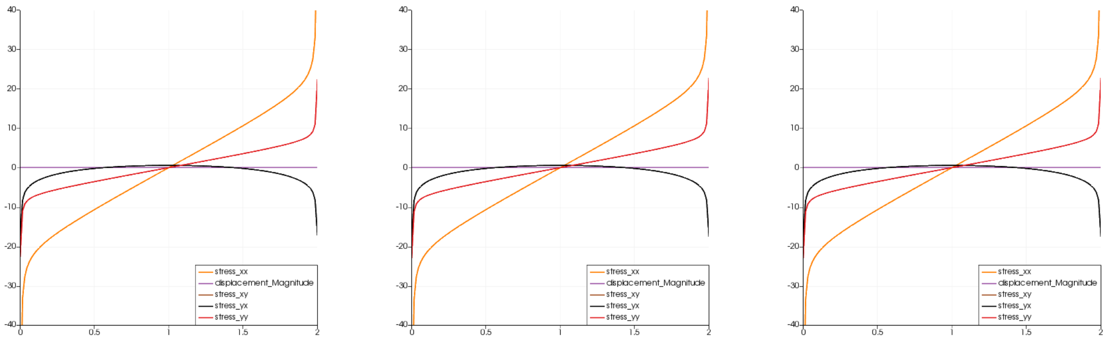

Q_2 $\qquad$ Q_2−gauss2 $\qquad$ Q_2

Figure 5.8: Plots of displacements and stresses on left edge of Timoshenko beam.

The Q_2-based methods give more accurate values (and more extreme stress values at the corners of the beam) than the Q_1 based elements, which is to be expected. One can see that the values in all the plots are similar, and check that they match those in [10].

Our methods produce correct plots using adaptive refinement [23] as well. By way of example, we provide a plot made using a Kelly error estimator [35] with our Q_2−gauss2 method in Figure 5.9, which also shows the adaptively refined mesh. As in [10], the adaptive refinement occurs mainly in the corners, since we have singular stress values there from fixing the beam's left edge at $\mathbf{u} = 0$, but giving the top and bottom boundaries Neumann conditions.

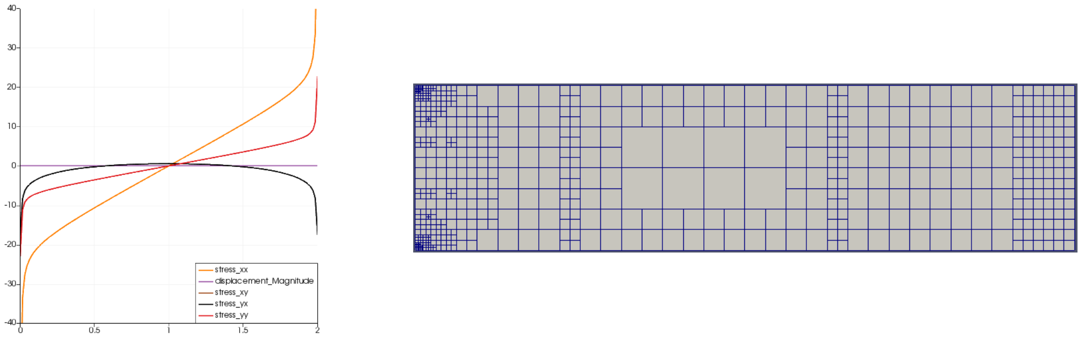

Figure 5.9: Q_2−gauss2 with adaptively refined mesh.

5.3 Locking revisited with non-standard methods

In Chapter 3 we showed that the standard Q_1 and Q_2 finite elements exhibit locking when modeling a nearly incompressible Timoshenko beam. We demonstrate in this section that our reduced-integration methods and our displacement-pressure methods, in addition to satisfying conventional error rates and matching a Timoshenko benchmark, cure locking.

5.3.1 Q_1-midpoint Timoshenko beam results

We first present visualizations of the Q_1-midpoint solutions on our Timoshenko beam setup in Figures 5.10 and 5.11.

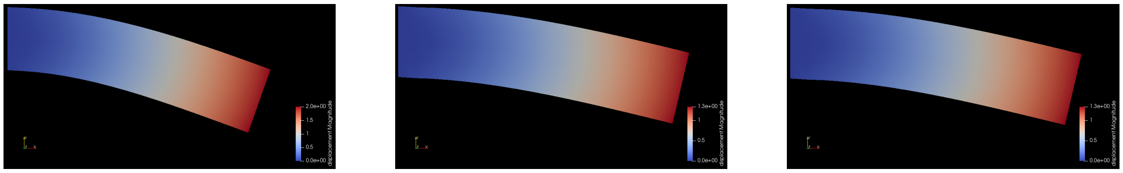

$\mu = 100, \lambda = 100$ $\mu = 100, \lambda = 5 \times 10^4$ $\mu = 100, \lambda = 5 \times 10^5$

Figure 5.10: Q_1-midpoint coarse mesh solutions.

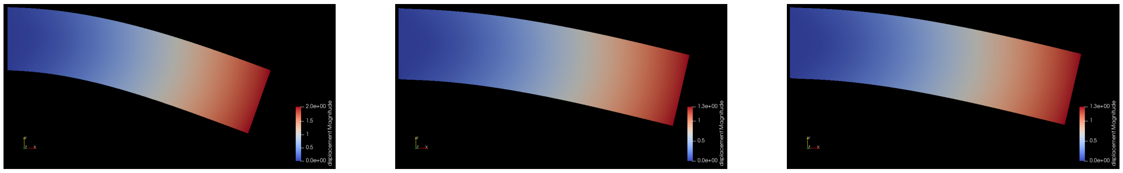

$\mu = 100, \lambda = 100$ $\mu = 100, \lambda = 5 \times 10^4$ $\mu = 100, \lambda = 5 \times 10^5$

Figure 5.11: Q_1-midpoint fine mesh solutions.

Note that the displacements on the coarse mesh and those on the fine mesh appear identical. We also provide Table 5.7 for a more in-depth analysis.

$\mathbf{Q_1}$−midpoint ($\mu = 100$)			
	$\lambda = 100$,	$\lambda = 5 \times 10^4$,	$\lambda = 5 \times 10^5$,
h	$\nu = 0.25$	$\nu = 0.499$	$\nu = 0.4999$
0.707107	-1.97755	-1.31344	-1.31082
0.353553	-1.99575	-1.31774	-1.31515
0.176777	-2.00113	-1.32197	-1.31941
0.0883883	-2.00277	-1.32439	-1.32185
0.0441942	-2.00329	-1.32561	-1.32308
Extrapolated	-2.00357	-1.32685	-1.32437
Relative difference	0.01299	0.01011	0.01023

Table 5.7: Q_1−midpoint solution values and relative differences for decreasing h

Note that the displacements on the coarse and fine mesh are much closer in the nearly incompressible cases (and are closer even in the reference case) than they are for the Q_1 element. Also notice that the relative errors are independent of λ and ν. Thus, we have shown our Q_1−midpoint element to solve the locking exhibited in the Q_1 element. (Note: Here we borrow the extrapolated exact error from the Q_2 method, since as we discussed previously, we expect our standard methods to eventually converge to the correct displacement given small enough values of h. We choose Q_2 over Q_1 for our extrapolation since Q_2 is the more accurate finite element.)

5.3.2 Q_2−gauss2 Timoshenko beam results

Figures 5.12 and 5.13 show our Q_2−gauss2 solutions on our Timoshenko beam setup.

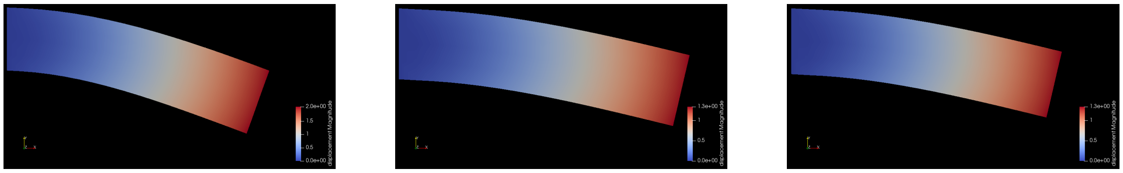

$\mu = 100, \lambda = 100$ $\mu = 100, \lambda = 5 \times 10^4$ $\mu = 100, \lambda = 5 \times 10^5$

Figure 5.12: Q_2−gauss2 coarse mesh solutions.

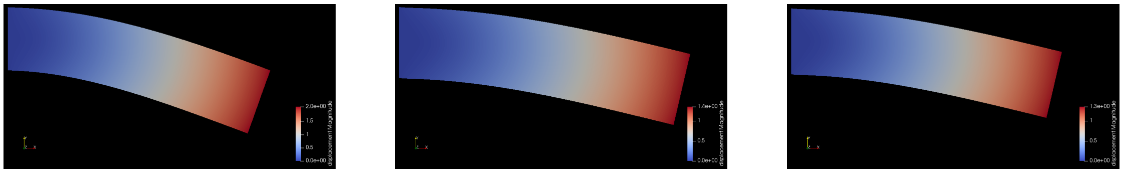

$\mu = 100, \lambda = 100$ $\mu = 100, \lambda = 5 \times 10^4$ $\mu = 100, \lambda = 5 \times 10^5$

Figure 5.13: Q_2−gauss2 fine mesh solutions.

Note that again, the beam moves the same amount on both the fine and the coarse mesh. Table 5.8 shows the values of the Q_2−gauss2 displacement for different values of h.

$\mathbf{Q_2}$−gauss2 ($\mu = 100$)			
	$\lambda = 100$, $\nu = 0.25$	$\lambda = 5 \times 10^4$, $\nu = 0.499$	$\lambda = 5 \times 10^5$, $\nu = 0.4999$
h			
0.707107	-2.00172	-1.31763	-1.31505
0.353553	-2.00289	-1.32291	-1.32035
0.176777	-2.0033	-1.32503	-1.32248
0.0883883	-2.00346	-1.32594	-1.32341
0.0441942	-2.00351	-1.32635	-1.32382
Extrapolated	-2.00357	-1.32685	-1.32437
Relative difference	0.00092	0.00695	0.00704

Table 5.8: Q_2−gauss2 solution values and relative differences for decreasing h

The coarse- and fine-mesh displacements here are closer than the coarse- and fine-mesh displacements of the Q_2 solution. The relative errors here are also significantly better than the relative errors of the Q_2 element. Thus, this element cures the locking of the Q_2 element. (Once again, we use the Q_2 solutions to create our extrapolated exact value.)

5.3.3 $Q_1 - dGP_0$ Timoshenko beam results

As we expect, Figures 5.14 and 5.15 showing our $Q_1 - dGP_0$ solutions look remarkably similar to our Q_1-midpoint solutions.

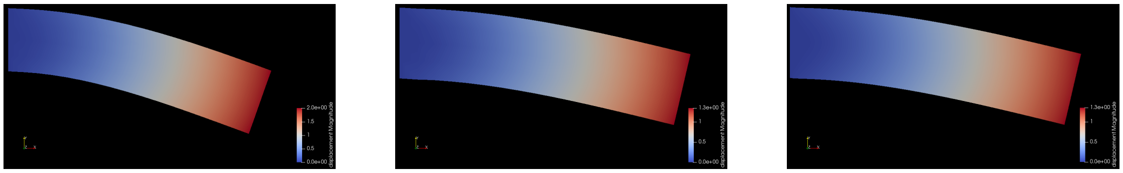

$\mu = 100, \lambda = 100$ $\mu = 100, \lambda = 5 \times 10^4$ $\mu = 100, \lambda = 5 \times 10^5$

Figure 5.14: $Q_1 - dGP_0$ coarse mesh solutions.

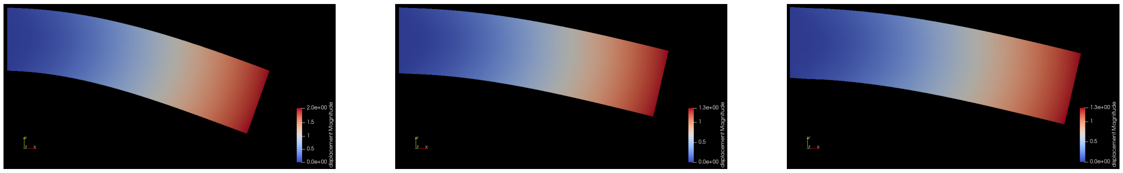

$\mu = 100, \lambda = 100$ $\mu = 100, \lambda = 5 \times 10^4$ $\mu = 100, \lambda = 5 \times 10^5$

Figure 5.15: $Q_1 - dGP_0$ fine mesh solutions.

Once again, these pictures show no locking.

As we have already demonstrated, the displacements in Table 5.9 are exactly the same as the Q_1-midpoint displacements for the same setup. Thus, this method too cures locking.

$\mathbf{Q_1 - dGP_0}$ $(\mu = 100)$			
	$\lambda = 100,$	$\lambda = 5 \times 10^4,$	$\lambda = 5 \times 10^5,$
h	$\nu = 0.25$	$\nu = 0.499$	$\nu = 0.4999$
0.707107	-1.97755	-1.31344	-1.31082
0.353553	-1.99575	-1.31774	-1.31515
0.176777	-2.00113	-1.32197	-1.31941
0.0883883	-2.00277	-1.32439	-1.32185
0.0441942	-2.00329	-1.32561	-1.32308
Extrapolated	-2.00357	-1.32685	-1.32437
Relative difference	0.01299	0.01011	0.01023

Table 5.9: $Q_1 - dGP_0$ solution values and relative differences for decreasing h

5.3.4 $Q_2 - dGP_1$ Timoshenko beam results

Figures 5.16 and 5.17 show that the $Q_2 - dGP_1$ also does not exhibit locking.

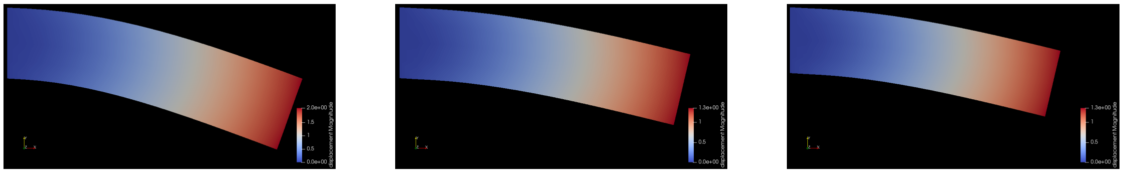

$\mu = 100, \lambda = 100$ $\mu = 100, \lambda = 5 \times 10^4$ $\mu = 100, \lambda = 5 \times 10^5$

Figure 5.16: $Q_2 - dGP_1$ coarse mesh solutions.

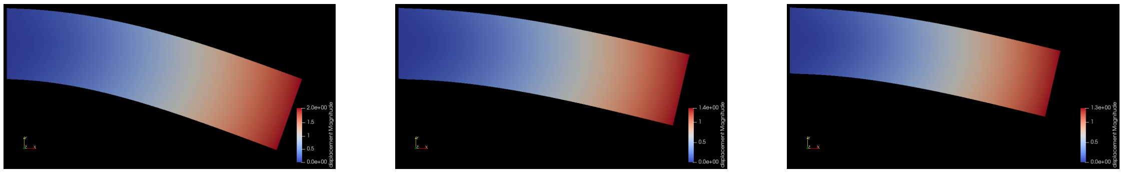

$\mu = 100, \lambda = 100$ $\mu = 100, \lambda = 5 \times 10^4$ $\mu = 100, \lambda = 5 \times 10^5$

Figure 5.17: $Q_2 - dGP_1$ fine mesh solutions.

Table 5.10 also shows no locking. The coarse- and fine-mesh displacements are closer than they are for the Q_2 element, and the relative errors here are better. (Note that these values are not, however, the same as the Q_2−gauss2 values.)

$\mathbf{Q_2 - dGP_1}$ $(\mu = 100)$			
	$\lambda = 100,$	$\lambda = 5 \times 10^4$	$\lambda = 5 \times 10^5$
h	$\nu = 0.25$	$\nu = 0.499$	$\nu = 0.4999$
0.707107	-2.0019	-1.32095	-1.31841
0.353553	-2.00295	-1.32428	-1.32175
0.176777	-2.00332	-1.32561	-1.32307
0.0883883	-2.00346	-1.3262	-1.32367
0.0441942	-2.00352	-1.32646	-1.32393
Extrapolated	-2.00357	-1.32685	-1.32437
Relative difference	0.00083	0.00445	0.00450

Table 5.10: $Q_2 - dGP_1$ solution values and relative differences for h decreasing.

5.4 Results summary

We can summarize our findings with displacement and error plots for each of our sets of parameter values. In the following plots of the displacement, the absolute values of the y-displacements of the point $(8, -1)$ are plotted against $1/h$ (proportional to the square root of number of cells in the mesh).

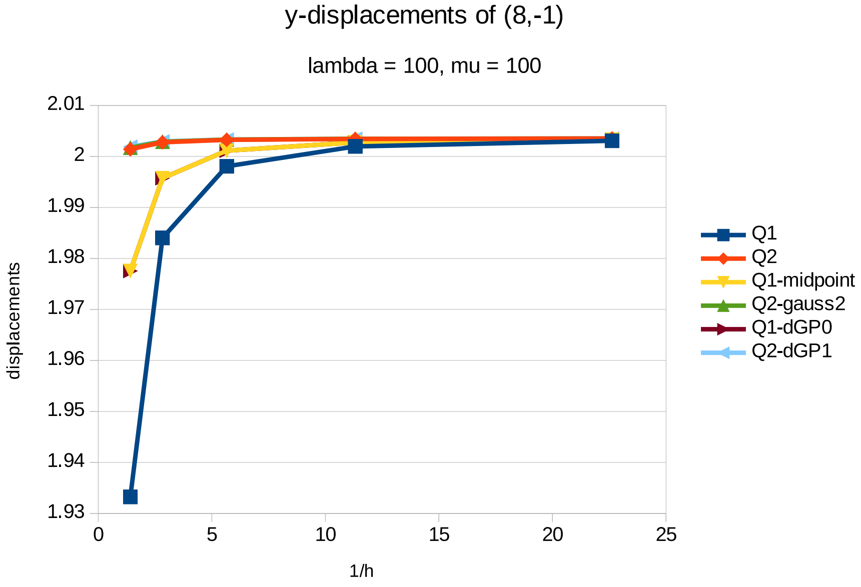

Figure 5.18: y-displacements of the point $(8, -1)$.

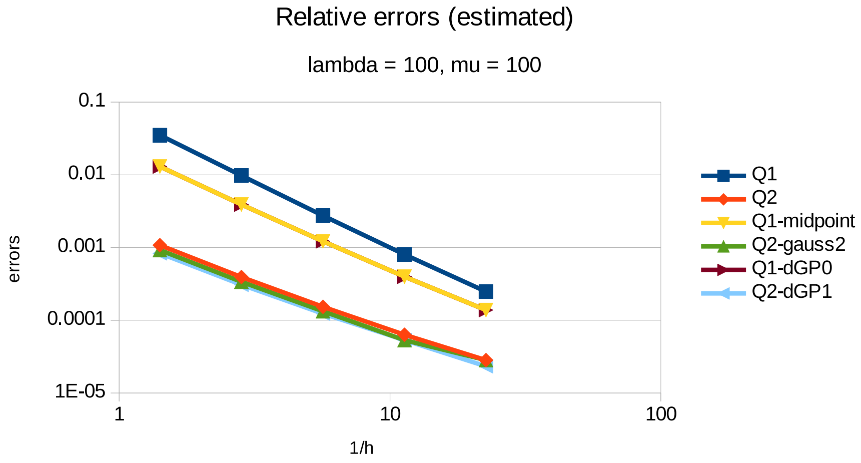

Figure 5.19: Relative estimated errors for y-displacements of the point $(8, -1)$

Even in the reference case with $\lambda = \mu = 100$ and $\nu = 0.25$, Q_1 is less accurate than Q_1-midpoint and $Q_1 - dGP_0$. Q_2 and Q_2-gauss2 are about equally accurate (Q_2-gauss2 is perhaps slightly better).

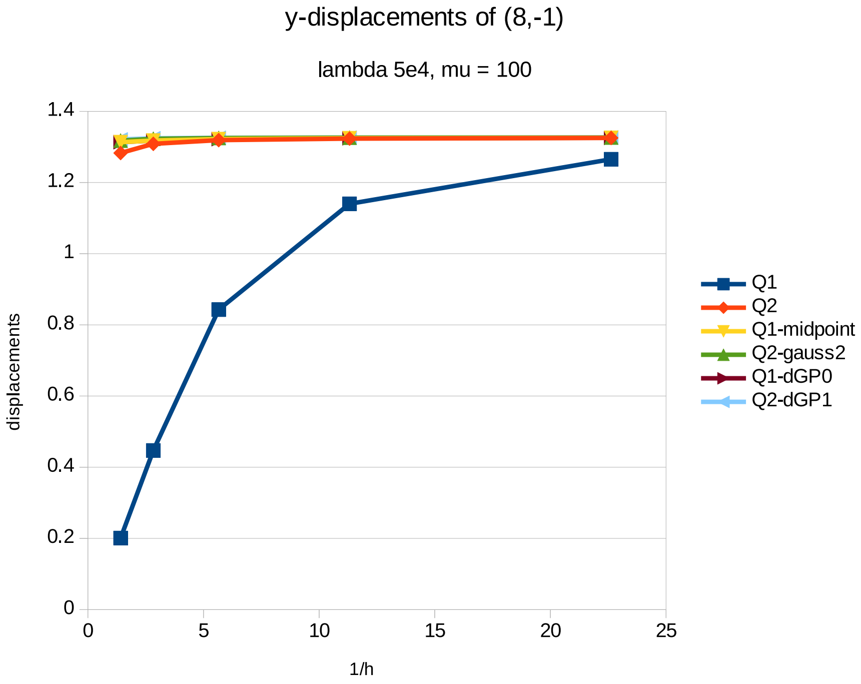

Figure 5.20: y-displacements of the point $(8, -1)$

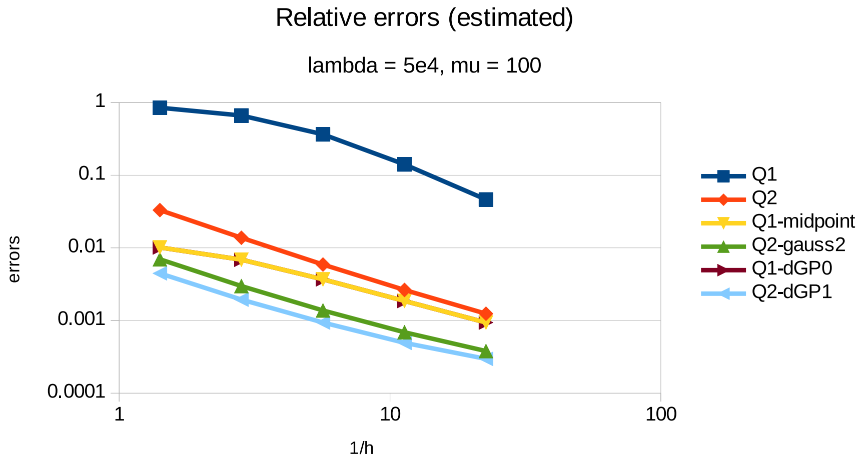

Figure 5.21: Relative estimated errors for the y-displacement of the point $(8, -1)$.

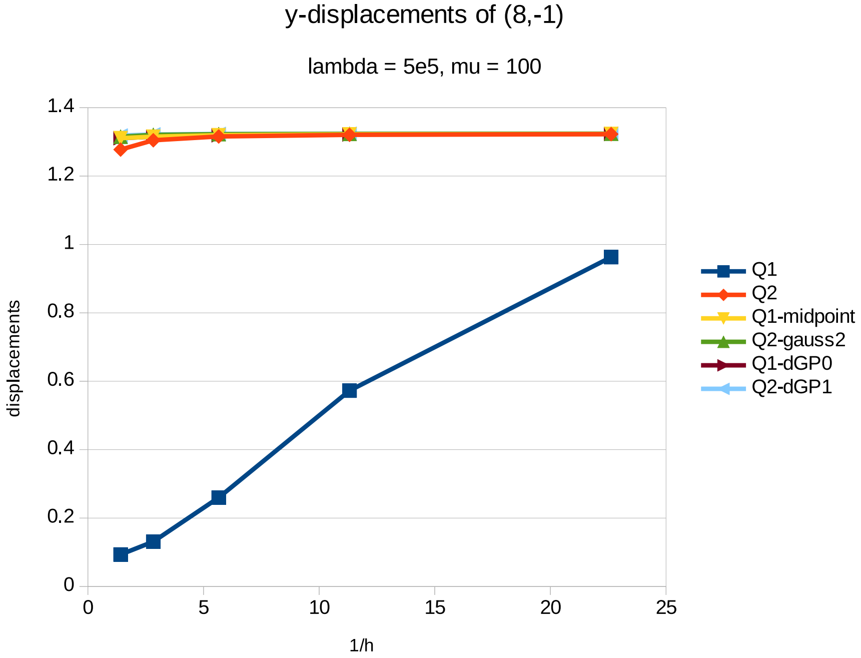

Figure 5.22: y-displacements of the point $(8, -1)$

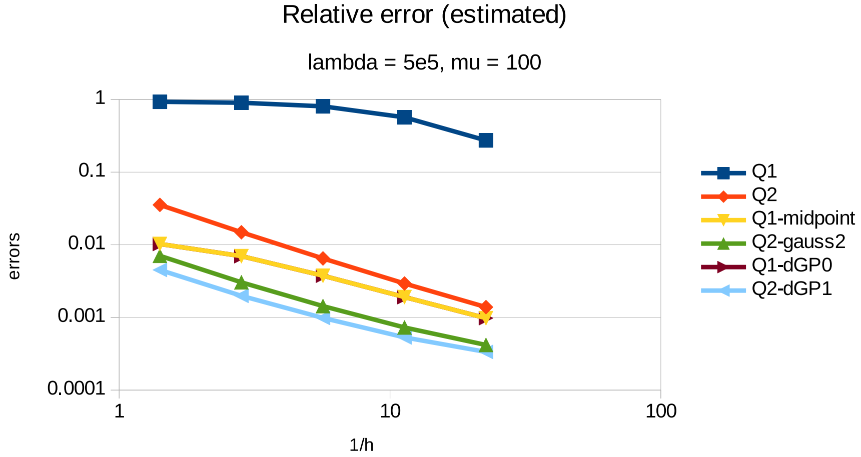

Figure 5.23: Relative estimated errors for the y-displacement of the point $(8, -1)$.

We see that the Q_1 relative errors are much worse than those of the non-standard methods, and that the non-standard methods have better relative errors than those of Q_2.

We can also see that the standard elements' relative errors increase more as the material becomes more nearly incompressible than do the non-standard elements' relative errors. By way of example, in Figures 5.24 and 5.25 we compare the relative errors of Q_1 and Q_1-midpoint and of Q_2 and Q_2-gauss2 as λ increases.

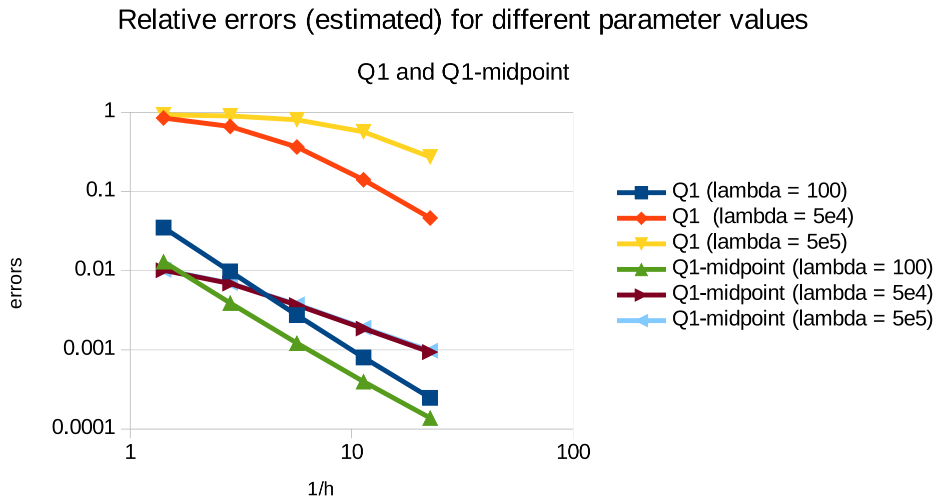

Figure 5.24: Relative estimated errors for the y-displacement of the point $(8, -1)$, for $\lambda = 100, 5 \times 10^4$, and 5×10^5.

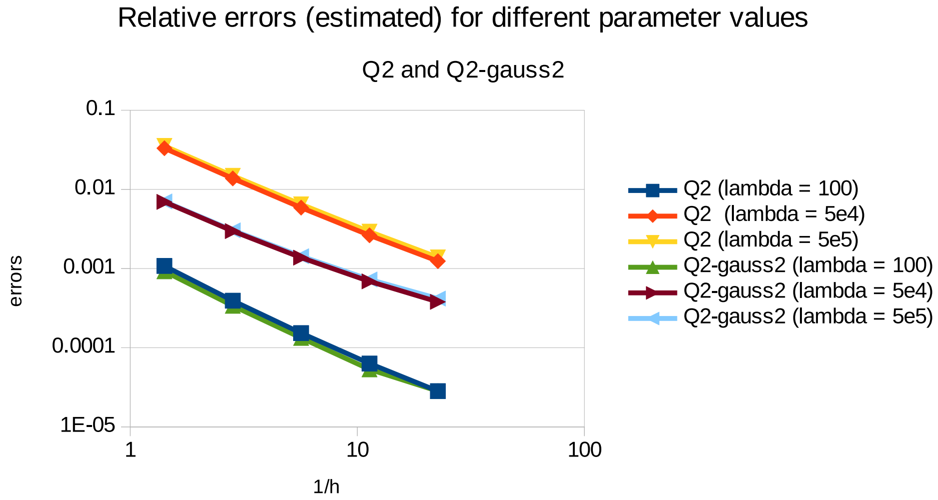

Figure 5.25: Relative estimated errors for the y-displacement of the point $(8, -1)$, for $\lambda = 100, 5 \times 10^4$, and 5×10^5.

In summary, for the incompressible cases, we see that the Q_1 element exhibits severe locking, and the Q_2 element also exhibits some locking. The relative errors of all of our non-standard methods are clearly better than either of the standard methods.

Chapter 6

Conclusions and Discussion

We first discussed the mathematical background for linear elasticity theory. We then derived the pure displacement weak form of linear elasticity, and presented the displacement-pressure formulation. Next, we introduced finite elements and presented a discretized formulation of our pure displacement formulation.

We next described locking as a phenomenon that occurs in nearly incompressible materials (λ large or ν close to $\frac{1}{2}$) for standard finite elements. We presented the reduced-integration methods Q_1-midpoint and Q_2-gauss2 and the displacement-pressure methods $Q_1 - dGP_0$ and $Q_2 - dGP_1$, and found that they solve the locking problem. Our findings can be summarized in Table 6.1.

	DoFs per cell	Error rates (manufactured solution)			Matches Timoshenko benchmark	Solves locking
		$[L^2(\Omega)]^d$	$[H^1(\Omega)]^d$	Optimal?		
Q_1	8	2	1	Yes	Yes	No
Q_2	18	3	2	Yes	Yes	No
Q_1-midpoint	8	2	1	Yes	Yes	Yes
Q_2-gauss2	18	3	2	Yes	Yes	Yes
$Q_1 - dGP_0$	8+1	2	1	Yes	Yes	Yes
$Q_2 - dGP_1$	18+3	3	2	Yes	Yes	Yes

Table 6.1: Summary of results.

Future work could include testing additional reduced-integration methods, solving problems on a non-rectangular mesh, further exploration of using reduced-integration techniques with adaptive refinement, and comparing the computational cost of the displacement-pressure methods and the reduced-integration techniques.

Appendices

Appendix A Link to code

Our implementations of our reduced-integration and displacement-pressure methods can be found at the following link.

`https://github.com/mathgirl/Linear_Elasticity`

Bibliography

[1] “Elasticity: Stress and strain,” 2018. [Online]. Available: https://opentextbc.ca/physicstestbook2/chapter/elasticity-stress-and-strain/

[2] J. Guermond and A. Ern, *Theory and Practice of Finite Elements.* Springer, 2004.

[3] D. Braess, *Finite Elements: Theory, fast solvers, and applications in solid mechanics.* Cambridge University Press, 2007.

[4] X.-l. Cheng, H.-c. Huang, and J. Zou, “Quadrilateral finite elements for planar linear elasticity problem with large lamé constant,” *Journal of Computational Mathematics*, pp. 357–366, 1998.

[5] H. R. Bayat, S. Wulfinghoff, S. Kastian, and S. Reese, “On the use of reduced integration in combination with discontinuous galerkin discretization: application to volumetric and shear locking problems,” *Advanced Modeling and Simulation in Engineering Sciences*, vol. 5, no. 1, p. 10, 2018.

[6] D. S. Malkus and T. J. Hughes, “Mixed finite element methodsreduced and selective integration techniques: a unification of concepts,” *Computer Methods in Applied Mechanics and Engineering*, vol. 15, no. 1, pp. 63–81, 1978.

[7] A. F. Bower, *Applied mechanics of solids.* CRC press, 2009.

[8] D. Boffi, F. Brezzi, and M. Fortin, “Finite elements for the stokes problem,” in *Mixed finite elements, compatibility conditions, and applications.* Springer, 2008, pp. 45–100.

[9] W. Bangerth, “The step-8 tutorial program,” 2018. [Online]. Available: https://www.dealii.org/9.0.0/doxygen/deal.II/step_8.html

[10] C. E. Augarde and A. J. Deeks, “The use of timoshenko’s exact solution for a cantilever beam in adaptive analysis,” *Finite elements in analysis and design*, vol. 44, no. 9-10, pp. 595–601, 2008. [Online]. Available: https://doi.org/10.1016/j.finel.2008.01.010

[11] "Linear elasticity," 2018. [Online]. Available: https://en.wikipedia.org/wiki/Linear_elasticity

[12] "Isotropic solid," 2017. [Online]. Available: https://en.wikipedia.org/wiki/Isotropic_solid

[13] "Homogeneity (physics)," 2017. [Online]. Available: https://en.wikipedia.org/wiki/Homogeneity_(physics)

[14] "Lamé parameters," 2018. [Online]. Available: https://en.wikipedia.org/wiki/Lam%C3%A9_parameters

[15] C. Johnson, *Numerical Solution of Partial Differential Equations by the Finite Element Method.* Dover Publications, Inc., 2009.

[16] S. Brenner and L. Scott, *The Mathematical Theory of Finite Element Methods.* Springer, 2002.

[17] F.-J. Sayas, "A gentle introduction to the finite element method," 2008. [Online]. Available: http://arturo.imati.cnr.it/~marini/didattica/Metodi-engl/Intro2FEM.pdf

[18] H. Lee, "Lecture notes for finite element methods," 2018.

[19] G. Kanschat, "Mixed finite element methods," 2017. [Online]. Available: http://www.mathsim.eu/~gkanscha/notes/mixed.pdf

[20] W. Bangerth, "Lecture 4: The building blocks of a finite element code," 2013. [Online]. Available: http://www.math.colostate.edu/~bangerth/videos.676.4.html

[21] T. Heister, "Lecture notes for data structures," 2017.

[22] W. Bangerth, "The step-6 tutorial program," 2018. [Online]. Available: https://www.dealii.org/9.0.0/doxygen/deal.II/step_6.html

[23] W. Bangerth and O. Kayser-Herold, "Data structures and requirements for hp finite element software," *ACM Transactions on Mathematical Software (TOMS)*, vol. 36, no. 1, p. 4, 2009.

[24] A. Bower, "Continuum mechanics: Mechanics of elastic solids," 2016. [Online]. Available: https://www.brown.edu/Departments/Engineering/Courses/En221/Notes/Elasticity/Elasticity.htm

[25] D. Braess and P. Ming, "A finite element method for nearly incompressible elasticity problems," *Mathematics of Computation*, vol. 74, no. 249, pp. 25–52, 2005.

[26] L. R. Herrmann, “Elasticity equations for incompressible and nearly incompressible materials by a variational theorem.” *AIAA journal*, vol. 3, no. 10, pp. 1896–1900, 1965.

[27] K.-S. Yun, J.-B. Park, G.-D. Jung, and S.-K. Youn, “Viscoelastic constitutive modeling of solid propellant with damage,” *International Journal of Solids and Structures*, vol. 80, pp. 118–127, 2016.

[28] G. B. L. C. Ahrens, James, *ParaView: An End-User Tool for Large Data Visualization,* Visualization Handbook. Elsevier, 2005.

[29] G. Alzetta, D. Arndt, W. Bangerth, V. Boddu, B. Brands, D. Davydov, R. Gassmoeller, T. Heister, L. Heltai, K. Kormann, M. Kronbichler, M. Maier, J.-P. Pelteret, B. Turcksin, and D. Wells, “The `deal.II` library, version 9.0,” *Journal of Numerical Mathematics*, 2018, accepted.

[30] W. Bangerth, R. Hartmann, and G. Kanschat, “deal.II – a general purpose object oriented finite element library,” *ACM Trans. Math. Softw.*, vol. 33, no. 4, pp. 24/1–24/27, 2007.

[31] M. Allmaras, “The step-29 tutorial program,” 2018. [Online]. Available: https://www.dealii.org/9.0.0/doxygen/deal.II/step_29.html

[32] W. Bangerth, “The step-7 tutorial program,” 2018. [Online]. Available: https://www.dealii.org/9.0.0/doxygen/deal.II/step_7.html

[33] ——, “The step-22 tutorial program,” 2018. [Online]. Available: https://www.dealii.org/9.0.0/doxygen/deal.II/step_22.html

[34] T. A. Davis, “Algorithm 832: Umfpack v4. 3—an unsymmetric-pattern multifrontal method,” *ACM Transactions on Mathematical Software (TOMS)*, vol. 30, no. 2, pp. 196–199, 2004.

[35] D. W. Kelly, J. P. De S. R. Gago, and I. Zienkiewicz, O. C.and Babuška, “A posteriori error analysis and adaptive processes in the finite element method: Part I–error analysis,” *Int. J. Num. Meth. Engrg.*, vol. 19, pp. 1593–1619, 1983.

Acknowledgments

Many thanks to Dr. Timo Heister for all of his time, and his directions, patient explanations, and instructive corrections. Thank you as well to the authors of the deal.II finite element library, upon which I have based my work. Finally, my thanks to Thomas Clevenger for all his help, and for his constant willingness to answer my many questions.